2

Deep inelastic scattering

In this chapter we present the cornerstones of perturbative QCD: the parton model of deep inelastic scattering (DIS) and the Dokshitzer–Gribov–Lipatov–Altarelli–Parisi (DGLAP) evolution equations. There exists an extensive literature covering these subjects using Lorentz-covariant Feynman diagram techniques (see the further reading section at the end of the chapter). Here we deviate from the traditional treatment and derive both the parton model and the DGLAP equations using light cone perturbation theory (LCPT). We argue that the light cone approach provides an intuitively clear space–time picture of the scattering process, which is universally applicable for high energy scattering. Owing to this universality, both the LCPT techniques used here and their space–time interpretation will prove very useful in subsequent chapters.

2.1 Kinematics, cross section, and structure functions

One of the simplest scattering processes that occur at short distances is the reaction

$$e + p \longrightarrow e' + X, \qquad (2.1)$$

known as deep inelastic electron–proton scattering (DIS). Here e and e' are the incoming and outgoing electron (or positron), p is the proton, and X stands for the other produced particles. The process is illustrated diagrammatically in Fig. 2.1 in the rest frame of the proton. The electron scatters on the proton through the exchange of a virtual photon (denoted γ^*) with a quark in the proton's wave function. The virtual photon usually breaks the proton apart, leading to the production of several new hadrons; these are labeled X in Fig. 2.1. Hence the process is deeply inelastic, which explains its name.

We begin by working in the rest frame of the proton. As shown in Fig. 2.1, the four-momentum of the proton is $P^\mu = (m, \vec{0})$, where m is the proton's mass. The four-momentum of the incoming electron is $p^\mu = (E, \vec{p})$, while the outgoing electron has four-momentum $p'^\mu = (E', \vec{p}')$. Out of the three independent four-momenta P^μ, p^μ, and p'^μ one can construct three Lorentz invariants relevant to the collision dynamics. (Note that $P^2 = m^2$ and $p^2 = p'^2 = m_e^2$, where m_e is the electron's mass; while these masses are indeed Lorentz scalars they do not carry any information about the scattering.) In terms of the virtual photon's four-momentum $q^\mu \equiv p^\mu - p'^\mu$, the three invariants usually employed to describe
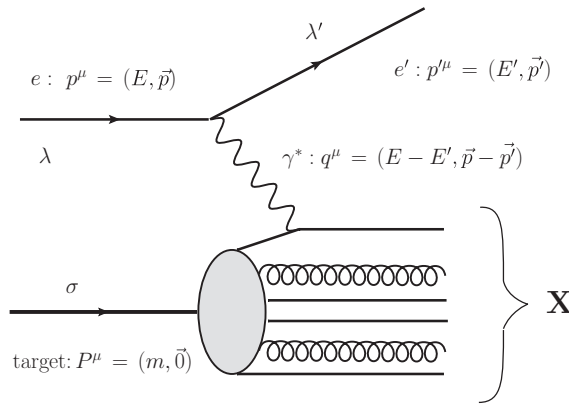
22

Fig. 2.1. Feynman diagram describing deep inelastic electron–proton scattering. The momentum labels of the lines correspond to the frame in which the target proton is at rest. The wavy line denotes the virtual photon propagator while the corkscrew lines denote the gluons inside the proton.

DIS are

$$Q^2 \equiv -q^2,$$
$$x_{Bj} \equiv \frac{Q^2}{2P \cdot q}, \tag{2.2}$$
$$y \equiv \frac{P \cdot q}{P \cdot p}.$$

The quantity Q^2 is called the virtuality of the photon, while x_{Bj} is the Bjorken-x variable. In the rest frame of the proton one can easily show that

$$Q^2 = 4E E' \sin^2 \frac{\theta}{2} \tag{2.3}$$

and

$$y = \frac{E - E'}{E}. \tag{2.4}$$

Here θ is the electron scattering angle, i.e., the angle between $\vec{p}$ and $\vec{p}\,'$. We therefore see that $q^2 \leq 0$ or, equivalently, $Q^2 \geq 0$, which demonstrates that Q is indeed real. In the proton's rest frame the third Lorentz invariant y has a physical interpretation as the fraction of the electron's energy transferred to the proton.

Apart from the three independent invariants in Eq. (2.2) one usually defines other Lorentz-invariant (but not independent) quantities,

$$\nu \equiv \frac{P \cdot q}{m} = E - E',$$
$$\hat{s} \equiv (P + q)^2 = 2P \cdot q + q^2 + m^2, \tag{2.5}$$
$$s \equiv (P + p)^2.$$

We see that in the proton's rest frame the invariant ν stands for that part of the electron's energy that is transferred to the proton; s denotes the center-of-mass energy squared of the electron scattering on the proton, while $\hat{s}$ is the center-of-mass energy squared of the $\gamma^* + p$ reaction. The invariants in Eq. (2.5) are related to those in Eq. (2.2) via

$$
\begin{aligned}
x_{Bj} &= \frac{Q^2}{\hat{s} + Q^2 - m^2} = \frac{Q^2}{2m\nu}, \\
Q^2 &= y x_{Bj}(s - m^2 - m_e^2) \approx y x_{Bj} s.
\end{aligned}
\tag{2.6}
$$

The fact that DIS experiments are usually performed at very high energy $s \gg m^2 \gg m_e^2$ justifies the approximation in the last line of Eq. (2.6). We also see from Eq. (2.6) that $x_{Bj} \leq 1$ for DIS on a proton.

The DIS experiment allows us to investigate the structure of the hadron at short distances by observing the recoil electron e' in Eq. (2.1). As we will see shortly, a DIS experiment can be thought of as a relativistic electron microscope. We can characterize this "microscope" by its maximal resolution. We will show below that with this DIS microscope we can resolve the sizes of the proton's constituents down to $1/Q$. Thus the physical meaning of the photon virtuality Q^2 is that it is related to the resolution of our "microscope". However, because our microscope is relavistic, we need to introduce one more variable, namely, the time duration of the observation. The number of particles is not conserved in a relativistic system: the number of quarks and gluons inside the proton constantly fluctuates owing to particle splitting and annihilation. Some fluctuations have longer lifetimes while others have shorter lifetimes. Therefore, the number of proton constituents can be different when measured over different observation times. We will show below that the measuring time of the DIS microscope is proportional to $1/x_{Bj}$, so that $t \sim 1/(m x_{Bj})$. This gives one of the two physical interpretations of x_{Bj}.

Using the covariant gauge for the photon propagator we can write the amplitude for the DIS process pictured in Fig. 2.1 as

$$
i M_{\sigma, \lambda, \lambda'}(X) = \frac{i e^2}{q^2} \, \bar{u}_{\lambda'}(p') \, \gamma_\mu \, u_\lambda(p) \, \langle X | J^\mu(0) | P, \sigma \rangle.
\tag{2.7}
$$

Here λ and λ' are the electron polarizations before and after the interaction and σ is the polarization of the proton (see Fig. 2.1). The initial state of the proton is denoted $|P, \sigma\rangle$, while the final state of the many produced hadrons X in Fig. 2.1 is correspondingly denoted as $|X\rangle$. We define the quark electromagnetic current by

$$
J^\mu(x) = \sum_f Z_f \, \bar{q}^f(x) \, \gamma^\mu \, q^f(x),
\tag{2.8}
$$

where Z_f is the quark's electric charge in units of the electron charge e, $q^f(x)$ is the quark field operator, and the sum in Eq. (2.8) runs over all quark flavors. (All operators in the book are in the Heisenberg representation.)

To calculate the total DIS cross section we need to square the amplitude (2.7), integrate or sum over the final-state quantum numbers, average over the initial-state quantum numbers, divide by the flux factor, and impose energy–momentum conservation (see e.g. Peskin and
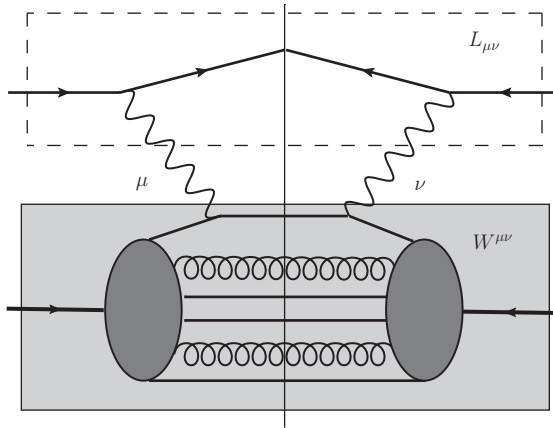
Fig. 2.2. Diagrammatic representation of the DIS cross section calculation as the amplitude squared. The vertical solid line denotes the final-state cut. The rectangular boxes encompass the parts of the diagram contributing to the leptonic tensor $L_{\mu\nu}$ and the hadronic tensor $W^{\mu\nu}$.

Schroeder (1995)). We get

$$\sigma^{ep} = \int \frac{d^3 p'}{(2\pi)^3 \, 2E \, 2E'} \frac{1}{4} \sum_{\sigma,\lambda,\lambda'} \sum_X |M_{\sigma,\lambda,\lambda'}(X)|^2 \, (2\pi)^4 \, \delta^4(P + q - p_X). \qquad (2.9)$$

Here p_X denotes the net four-momentum of all the hadrons produced in the scattering process.

Without giving the details of the calculation, which can be found in standard textbooks (Halzen and Martin 1984, Peskin and Schroeder 1995, Sterman 1993), we will write down the following expression for the DIS cross section, which results from substituting Eq. (2.7) into Eq. (2.9):

$$\frac{d\sigma}{d^3 p'} = \frac{\alpha_{EM}^2}{E \, E' \, Q^4} \, L_{\mu\nu} W^{\mu\nu}. \qquad (2.10)$$

Equation (2.10) is illustrated in Fig. 2.2, which shows the amplitude from Fig. 2.1 squared. As shown graphically in Fig. 2.2, one can separate the electron and proton contributions to the DIS cross section into leptonic and hadronic parts. Formally, the leptonic part brings in a *leptonic tensor* $L_{\mu\nu}$, while the hadronic part yields a *hadronic tensor* $W^{\mu\nu}$.

From Eqs. (2.7) and (2.9) we can easily see that one defines the *leptonic tensor* by

$$L_{\mu\nu} = \frac{1}{2} \sum_{\lambda=\pm 1} \sum_{\lambda'=\pm 1} \bar{u}_{\lambda'}(p') \, \gamma_\mu \, u_\lambda(p) \left[\bar{u}_{\lambda'}(p') \, \gamma_\nu \, u_\lambda(p) \right]^*. \qquad (2.11)$$

Summing over the initial and final electron polarizations yields

$$\begin{aligned}
L_{\mu\nu} &= \frac{1}{2} \operatorname{Tr} \left[(\slashed{p}' + m_e) \, \gamma_\mu \, (\slashed{p} + m_e) \, \gamma_\nu \right] \\
&= 2 \left(p_\mu p'_\nu + p_\nu p'_\mu - p \cdot p' g_{\mu\nu} + m_e^2 \, g_{\mu\nu} \right),
\end{aligned} \qquad (2.12)$$

where again m_e is the electron mass.

The *hadronic tensor* $W^{\mu\nu}$ in Eq. (2.10) is given by

$$W^{\mu\nu} = \frac{1}{4\pi m} \frac{1}{2} \sum_{\sigma=\pm 1} \sum_X \langle P, \sigma | J^\mu(0) | X \rangle \langle X | J^\nu(0) | P, \sigma \rangle$$
$$\times (2\pi)^4 \delta^4(P + q - p_X), \tag{2.13}$$

which can be simplified to

$$W^{\mu\nu} = \frac{1}{4\pi m} \int d^4x \, e^{iq\cdot x} \frac{1}{2} \sum_{\sigma=\pm 1} \sum_X \langle P, \sigma | J^\mu(x) | X \rangle \langle X | J^\nu(0) | P, \sigma \rangle$$
$$= \frac{1}{4\pi m} \int d^4x \, e^{iq\cdot x} \frac{1}{2} \sum_{\sigma=\pm 1} \langle P, \sigma | J^\mu(x) J^\nu(0) | P, \sigma \rangle$$
$$\equiv \frac{1}{4\pi m} \int d^4x \, e^{iq\cdot x} \langle P | J^\mu(x) J^\nu(0) | P \rangle \tag{2.14}$$

where the last line defines an abbreviated notation for the spin-averaged proton state and m is the mass of the proton.

The strong interaction dynamics in DIS (including nonperturbative contributions) is entirely contained in the hadronic tensor $W^{\mu\nu}$; therefore, it is very hard to calculate $W^{\mu\nu}$ in a "first principles" QCD calculation. However, we can infer more about its structure by noting that conservation of the electromagnetic current (2.8) requires that

$$q_\mu W^{\mu\nu} = 0, \qquad q_\nu W^{\mu\nu} = 0. \tag{2.15}$$

Imposing the condition (2.15) on $W^{\mu\nu}$ and assuming that the tensor is symmetric one can show that, without loss of generality, it can be written in the following form (see Exercise 2.1 at the end of the chapter):

$$W^{\mu\nu} = - W_1(x_{Bj}, Q^2) \left(g^{\mu\nu} - \frac{q^\mu q^\nu}{q^2} \right)$$
$$+ \frac{W_2(x_{Bj}, Q^2)}{m^2} \left(P^\mu - \frac{P \cdot q}{q^2} q^\mu \right) \left(P^\nu - \frac{P \cdot q}{q^2} q^\nu \right). \tag{2.16}$$

Here W_1 and W_2 are unknown scalar functions of x_{Bj} and Q^2, called *structure functions*. As $W^{\mu\nu}$ describes the interaction of the virtual photon with the proton, there are only two four-momentum vectors on which it depends: P^μ and q^μ. As $P^2 = m^2$ one can construct only two Lorentz invariants from them that describe the scattering process. We will use x_{Bj} and Q^2 as the two invariants on which W_1 and W_2 depend.

Substituting Eq. (2.16) into Eq. (2.10), after some algebra one can show that the cross section of the reaction $e + p \to e' + X$ in terms of the functions W_1 and W_2 is (for details of the derivation see, for example, the book Halzen and Martin (1984), Chapter 8)

$$\frac{d\sigma^{ep}}{dE' \, d\Omega} = \frac{\alpha^2_{EM}}{4\,E^2\,\sin^4\frac{\theta}{2}} \left[W_2(x_{Bj}, Q^2) \cos^2\frac{\theta}{2} + 2W_1(x_{Bj}, Q^2) \sin^2\frac{\theta}{2} \right]. \tag{2.17}$$

In arriving at Eq. (2.17) we have neglected the mass of the electron m_e, to write

$$d^3 p' = p'^2 \, dp' \, d\Omega \approx E'^2 \, dE' \, d\Omega,$$

where Ω is the solid scattering angle. We have also used Eq. (2.3) to replace Q^2. Equation (2.17) demonstrates that the structure functions W_1 and W_2 can be measured experimentally by studying the angular dependence of the DIS cross section.

Note that the structure functions W_1 and W_2 have the dimension of inverse mass.[1] It is more convenient to define dimensionless structure functions F_1 and F_2, by

$$F_1(x_{Bj}, Q^2) \equiv m W_1(x_{Bj}, Q^2), \tag{2.18a}$$

$$F_2(x_{Bj}, Q^2) \equiv \nu W_2(x_{Bj}, Q^2) = \frac{Q^2}{2m x_{Bj}} W_2(x_{Bj}, Q^2). \tag{2.18b}$$

All the QCD physics in DIS is contained in F_1 and F_2. We will now attempt to calculate these structure functions.

2.2 Parton model and Bjorken scaling

To find the structure functions F_1 and F_2 it is easier to change the frame in which we are working. Instead of the proton's rest frame we will now use a frame in which the proton is ultrarelativistic. Such a frame is usually referred to as the *infinite momentum frame* (IMF) or Bjorken frame. The proton is taken to be moving along the z-axis, and its momentum in this frame is

$$P^\mu \approx \left(P + \frac{m^2}{2P}, 0, 0, P \right) \tag{2.19}$$

in the (P^0, P^1, P^2, P^3) notation. We assume that the proton's momentum is much larger than its mass, $P \gg m$. The virtual photon in the IMF has $q^3 = 0$, so that

$$q^\mu = (q^0, q^1, q^2, 0). \tag{2.20}$$

The part of the DIS process relevant for the calculation of the structure functions, virtual photon–proton scattering, is depicted in Fig. 2.3. Note that, unlike Fig. 2.2, we now draw the proton at the top of the diagram. In fact, in our normal convention a proton at rest (or any other target) is drawn at the bottom of the diagram, while a proton (or any other projectile) moving at high energy is shown at the top of the diagram.

2.2.1 Warm-up: DIS on a single free quark

As a warm-up calculation in preparation for the full *parton model*, let us simply assume that the proton consists of noninteracting quarks and gluons, which we will refer to as *partons*. As we will see below in Sec. 2.3, this is not such a bad approximation as in the IMF the

---

[1] Our single-particle states are normalized such that $\langle p | p' \rangle = (2\pi)^3 \, 2E_p \, \delta^3(\vec{p} - \vec{p}')$, which allows one to see that the dimension of $W^{\mu\nu}$ in Eq. (2.14) is that of inverse mass.
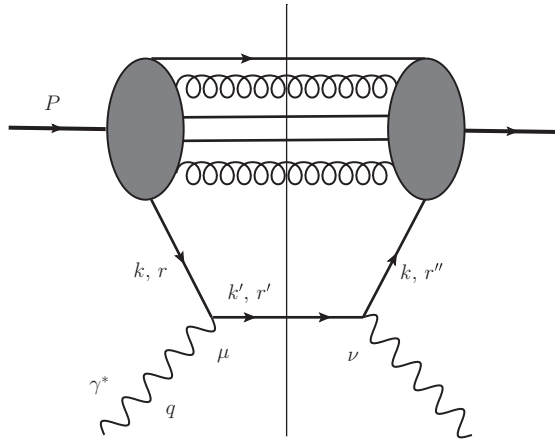
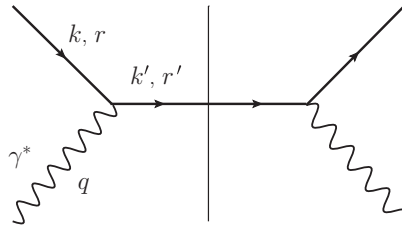Fig. 2.3. Virtual photon–proton scattering in the IMF.

Fig. 2.4. Interaction of a virtual photon with one point-like particle (a parton), as the basic ingredient of the parton model. As usual, the vertical solid line denotes the final-state cut.

typical time scale of the quark and gluon interactions inside the proton is much longer than the time scale of DIS. Hence for the duration of the virtual photon–proton scattering we can assume that the quarks and gluons do not interact with each other. Thus the photon simply interacts with a quark in the proton. To better understand photon–quark scattering let us assume that we simply have one free quark instead of the proton. The diagram giving the cross section of the DIS process is shown in Fig. 2.4.

The hadronic tensor $W_{\mu\nu}$ for the interaction of the virtual photon with the point-like particle (a single quark) has a structure similar to $L_{\mu\nu}$ in Eq. (2.11), namely

$$W_{\mu\nu}^{quark} = \frac{Z_f^2}{2} \sum_{r=\pm 1} \sum_{r'=\pm 1} \bar{u}_{r'}(k') \gamma_\mu u_r(k) \left[\bar{u}_{r'}(k') \gamma_\nu u_r(k) \right]^* \frac{1}{2m_q} \delta\left(k'^2 - m_q^2\right)$$

$$= \frac{Z_f^2}{2} \operatorname{Tr}\left[(\slashed{k}' + m_q)\gamma_\mu (\slashed{k} + m_q)\gamma_\nu \right] \frac{1}{2m_q} \delta\left(k'^2 - m_q^2\right), \tag{2.21}$$

where $k' = k + q$ while r and r' are the quark helicities (see Fig. 2.4) and m_q is the quark mass. Equation (2.21) can be obtained from Eq. (2.13) by replacing X in it by a single

particle (a quark), so that

$$\sum_{X=\text{one particle}} = \int \frac{d^3k'}{2k'^0\,(2\pi)^3}\sum_{r'=\pm 1}$$

along with $p_X \to k'$ and $P \to k$. It is then easy to show that

$$\frac{1}{4\pi m_q}\int \frac{d^3k'}{2k'^0\,(2\pi)^3}\,(2\pi)^4\,\delta^4(k+q-k') = \frac{1}{2m_q}\,\delta\left((k+q)^2 - m_q^2\right), \qquad (2.22)$$

justifying the delta function factor in Eq. (2.21).

We can rewrite $\delta((k+q)^2 - m_q^2)$ as follows:

$$\delta\left((k+q)^2 - m_q^2\right) = \delta\left(2k\cdot q - Q^2\right) = \frac{1}{2\,k\cdot q}\,\delta\left(1 - \frac{Q^2}{2\,k\cdot q}\right), \qquad (2.23)$$

where we have used the fact that the incoming quark is on mass shell.

Calculating the trace in Eq. (2.21), comparing the result with Eq. (2.16), and using Eqs. (2.18a) and (2.18b) with P replaced by k we obtain for DIS on a point-like particle (a quark)

$$F_1^{quark}\left(x_{Bj}, Q^2\right) = m_q W_1^{quark}\left(x_{Bj}, Q^2\right) = \frac{Z_f^2}{2}\,\delta\left(1 - x_{Bj}\right) \qquad (2.24)$$

$$F_2^{quark}\left(x_{Bj}, Q^2\right) = \frac{Q^2}{2m_q x_{Bj}}\,W_2^{quark}\left(x_{Bj}, Q^2\right) = Z_f^2\,\delta\left(1 - x_{Bj}\right). \qquad (2.25)$$

We have used the fact that, for DIS on a single quark, $x_{Bj} = Q^2/(2k\cdot q)$. We see that for DIS on a point-like particle the structure functions F_1 and F_2 turn out to depend only on one variable, x_{Bj}. This behavior is known as *Bjorken scaling* (Bjorken 1969).

2.2.2 Full calculation: DIS on a proton

The idea that the actual interaction in DIS occurs with the point-like constituents of a hadron (the partons) can be illustrated by studying the full DIS process. Let us consider DIS on the whole proton, as shown in Fig. 2.3. We want to calculate the diagram in Fig. 2.3 using the rules of light cone perturbation theory (LCPT) outlined in Sec. 1.3 (see also Sec. 1.4). We first rewrite all four-momenta in the light cone $(+, -, \perp)$ notation. In the IMF/Bjorken frame the proton has a very large momentum. The proton's momentum in Eq. (2.19) becomes, in light cone notation,

$$P^\mu \approx (P^+, 0, 0_\perp) \qquad (2.26)$$

with very large $P^+ \approx 2P$. Quarks and gluons in such an ultrarelativistic proton also have very large light cone plus momenta. The quark in Fig. 2.3 has four-momentum $k^\mu = (k^+, (\vec{k}_\perp^2 + m_q^2)/k^+, \vec{k}_\perp)$; we assume that it has a large k^+ component. We define the Feynman-x variable as the fraction of the light cone momentum of the proton carried by
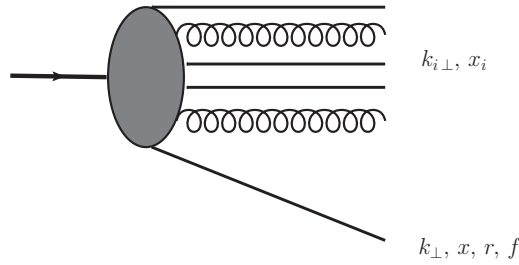
Fig. 2.5. Light cone wave function of the proton.

this quark[2]

$$x \equiv \frac{k^+}{P^+}, \tag{2.27}$$

writing $k^\mu = (x P^+, (\vec{k}_\perp^2 + m_q^2)/(x P^+), \vec{k}_\perp)$.

In LCPT every particle is on mass shell. However, we want to calculate the virtual photon–proton scattering cross section for the process shown in Fig. 2.3. By the definition of the problem the incoming photon is virtual, $q^2 = -Q^2$. Hence in LCPT we can treat this virtual photon as having an imaginary mass iQ. The virtual photon momentum (2.20) becomes, in light cone notation,

$$q^\mu = \left(q^+, \frac{\vec{q}_\perp^2 - Q^2}{q^+}, \vec{q}_\perp \right) \tag{2.28}$$

with $(q^+)^2 = \vec{q}_\perp^2 - Q^2$ in the IMF.

In the calculations below we will assume that Q^2 is very large. First, for QCD perturbation theory to be applicable Q^2 has to be much larger than the confinement scale Λ_{QCD}: $Q^2 \gg \Lambda_{QCD}^2$. Second, for the parton model (which we are about to present) to be valid, Q has to be much larger than the transverse momentum of any other particle in the problem. This applies to the quark line carrying momentum k in Fig. 2.3, for which we have $Q^2 \gg \vec{k}_\perp^2, m_q^2$. If, for a particular wave function configuration the upper boxed part of Fig. 2.3 contains n partons with transverse momenta $\vec{k}_{i\perp}$ for $i = 1, \ldots, n$, then we will assume that $Q^2 \gg \vec{k}_{i\perp}^2$ for any i. Note that $\vec{q}_\perp^2 = Q^2 + (q^+)^2 > Q^2$ is also very large.

Now let us assume that these n partons carry light cone momentum components k_i^+ or, equivalently, have Feynman-x values given by x_i for $i = 1, \ldots, n$. We can then define the light cone wave function of the $(n + 1)$-parton Fock state of the proton and denote it by $\Psi_n^f (\{x_i, k_{i\perp}\}; x, k_\perp; r)$. The proton has n "spectator" partons (both quarks and gluons) and one quark carrying momentum k in Fig. 2.3 that interacts with the photon. This quark has helicity r and flavor f. The light cone wave function $\Psi_n^f (\{x_i, k_{i\perp}\}; x, k_\perp; r)$ is illustrated in Fig. 2.5. In our discussion and notation we will suppress the polarization indices of the

---

[2] The Feynman-x variable was originally defined as $x = 2k^3/\sqrt{s}$ in the center-of-mass frame with k^μ the momentum of the produced outgoing particle (Feynman 1969). Our definition here is different, but is also widely used in the community: it maps back onto the original definition at large x.

proton and the polarization, color, and flavor indices of the spectator partons: averaging over the proton polarizations and summation over the polarization, color, and flavor of the partons will always be implicitly assumed to be made after we have multiplied the wave function $\Psi_n^f(\{x_i, k_{i\perp}\}; x, k_\perp; r)$ by its complex conjugate. Note also that $k_\perp = |\vec{k}_\perp|$ (the same notation applies to the other transverse momenta).

Let us now calculate the proton's $W_{\mu\nu}$ using Eq. (2.13). Note that after the interaction the n spectator partons, along with the quark that interacts with the photon, together form what is denoted X in Eq. (2.13). Therefore, for n partons we have (see also Eq. (1.67))

$$
\sum_{X = n \, \text{partons}} = \int \frac{dk'^+}{k'^+} \frac{d^2 k'_\perp}{2(2\pi)^3} \frac{1}{S_n} \sum_{r'=\pm 1} \prod_{i=1}^n \frac{dk_i^+}{k_i^+} \frac{d^2 k_{i\perp}}{2(2\pi)^3}
$$
$$
= \int \frac{dk'^+}{k'^+} \frac{d^2 k'_\perp}{2(2\pi)^3} \frac{1}{S_n} \sum_{r'=\pm 1} \prod_{i=1}^n \frac{dx_i}{x_i} \frac{d^2 k_{i\perp}}{2(2\pi)^3}, \tag{2.29}
$$

where for physical particles all integrals over the k_i^+ and k'^+ run from 0 to P^+, which translates into integrals over the x_i running from 0 to 1. Here $k'^+ = k^+ + q^+$, $\vec{k}'_\perp = \vec{k}_\perp + \vec{q}_\perp$, and r' is the helicity of the k' quark line (see Fig. 2.3). The symmetry factor S_n is defined after Eq. (1.67).

Following the definition of the hadronic tensor in Eq. (2.13) and with the help of the diagram in Fig. 2.3 we can write, using the LCPT rules presented in Secs. 1.3 and 1.4,

$$
W_{\mu\nu} = \frac{1}{4\pi m} \sum_{n, f} \int \frac{dk'^+ \, d^2 k'_\perp}{2k'^+ (2\pi)^3} \frac{1}{S_n} \sum_{r, r', r''} \prod_{i=1}^n \frac{dx_i}{x_i} \frac{d^2 k_{i\perp}}{2(2\pi)^3}
$$
$$
\times \frac{P^+}{k^+} \Psi_n^f(\{x_i, k_{i\perp}\}; x, k_\perp; r) \left[\frac{P^+}{k^+} \Psi_n^f(\{x_i, k_{i\perp}\}; x, k_\perp; r'') \right]^* Z_f^2
$$
$$
\times \bar{u}_{r'}(k') \gamma_\mu u_r(k) \left[\bar{u}_{r'}(k') \gamma_\nu u_{r''}(k) \right]^* (2\pi)^4 \delta^4 \left(P + q - k' - \sum_{j=1}^n k_j \right). \tag{2.30}
$$

The labeling of the quark helicities r, r', and r'' is defined in Fig. 2.3. Note that, unlike in the simple case of DIS on a single quark considered above, the helicity of the quark line k in Fig. 2.3 is different on the left and on the right of the final-state cut. The factors P^+/k^+ multiplying the wave functions in Eq. (2.30) appear for two reasons. A factor $1/k^+$, which has to be included by the rules of LCPT from Sec. 1.3, is due to the internal quark line carrying momentum k and is not included in our definition of the light cone wave function outlined in Sec. 1.4. The same definition from Sec. 1.4 dictates that each light cone wave function contains a factor $1/P^+$ for each incoming line but, as the general LCPT rules in Sec. 1.3 prescribe no such factor for the full diagram for the scattering process, we need to remove this factor by multiplying the wave functions by P^+.

The delta function in Eq. (2.30) imposes the conservation of the transverse and "+" components of momenta. However, of particular importance is the conservation of the light cone energy that is also imposed by this delta function. Using Eq. (2.26) and rewriting the

light cone energies of all partons in terms of the transverse and "+" components of their momenta we obtain

$$\frac{1}{k'^+} \delta\left(P^- + q^- - k'^- - \sum_{j=1}^{n} k_j^-\right)$$

$$= \frac{1}{k^+ + q^+} \delta\left(q^- - \frac{(\vec{k}_\perp + \vec{q}_\perp)^2}{k^+ + q^+} - \sum_{j=1}^{n} \frac{k_{j\perp}^2}{k_j^+}\right). \tag{2.31}$$

For simplicity we will now assume that all the partons are massless. This assumption also applies to the quark that interacts with the photon, for which we now put $m_q = 0$.

Since $Q^2, \vec{q}_\perp^2 \gg \vec{k}_\perp^2, k_{i\perp}^2$ for any i we approximate $(\vec{k}_\perp + \vec{q}_\perp)^2$ as $\vec{q}_\perp^2$ and also neglect all $k_{j\perp}^2/k_j^+$ in the argument of the delta function in Eq. (2.31). This leaves us with

$$\frac{1}{k^+ + q^+} \delta\left(q^- - \frac{(\vec{k}_\perp + \vec{q}_\perp)^2}{k^+ + q^+} - \sum_{j=1}^{n} \frac{k_{j\perp}^2}{k_j^+}\right) \approx \delta\big((k^+ + q^+)q^- - \vec{q}_\perp^2\big)$$

$$= \delta\big(k^+ q^- - Q^2\big) = \delta\big(x P^+ q^- - Q^2\big) \approx \delta\big(x \, 2P \cdot q - Q^2\big), \tag{2.32}$$

where the last approximation was made using Eq. (2.26). Using the definition of x_{Bj} the last delta function can be rewritten as

$$\delta\left(x \, 2P \cdot q - Q^2\right) = \frac{1}{2P \cdot q} \delta(x - x_{Bj}) = \frac{x_{Bj}}{Q^2} \delta(x - x_{Bj}). \tag{2.33}$$

We see that Feynman x is identical to Bjorken x. The physical meaning of x_{Bj} becomes clear: *it is the fraction of the light cone momentum of the proton carried by the struck quark!*

Since the two quantities are equal, below we will use x and x_{Bj} interchangeably, using the notation with a subscript (x_{Bj}) only in cases when we need to avoid the potential confusion of x with other quantities.

Using Eq. (2.33) in Eq. (2.30) and summing over the helicities r' yields

$$W_{\mu\nu} = \frac{1}{4m} \sum_{n,\,f} \int dk^+ d^2k_\perp \frac{1}{S_n} \sum_{r,r''} \prod_{i=1}^{n} \frac{dx_i}{x_i} \frac{d^2k_{i\perp}}{2(2\pi)^3}$$

$$\times \Psi_n^f\left(\{x_i, k_{i\perp}\}; \frac{k^+}{P^+}, k_\perp; r\right) \left[\Psi_n^f\left(\{x_i, k_{i\perp}\}; \frac{k^+}{P^+}, k_\perp; r''\right)\right]^* Z_f^2$$

$$\times \bar{u}_{r''}(k) \gamma_\nu \, (\slashed{k} + \slashed{q}) \, \gamma_\mu \, u_r(k) \, \delta\left(P^+ - k^+ - \sum_{l=1}^{n} k_l^+\right) \delta^2\left(\vec{k}_\perp + \sum_{j=1}^{n} \vec{k}_{j\perp}\right)$$

$$\times \left(\frac{P^+}{k^+}\right)^2 \frac{x_{Bj}}{Q^2} \delta\left(x_{Bj} - \frac{k^+}{P^+}\right), \tag{2.34}$$

where we have switched from integration variables k'^+ and $\vec{k}'_\perp$ to k^+ and $\vec{k}_\perp$.

An important assumption of the parton model is that the integrals in Eq. (2.34) are convergent even if we impose no integration limit on the transverse momentum integrals.

As will be shown below, this assumption is not true in QCD, where we have to cut off the $k_\perp$-integral at Q^2 in the ultraviolet (UV), which leads to corrections to the naive parton model presented in this section; the $k_\perp$-integral converges in the UV for a theory in which partons are scalars. For now we will not address this issue and simply assume that, owing to some (perturbative or nonperturbative) physics beyond our present formalism, the $k_\perp$-integral is convergent in the UV.

We can then see that all the integrals in Eq. (2.34) "know" only about one momentum external to the integration: that momentum is P. Hence writing $\slashed{k} + \slashed{q}$ from Eq. (2.34) as $(k + q)_\alpha \gamma^\alpha$ we can argue, on the basis of Lorentz transformation properties, that after all integrations in Eq. (2.34) have been carried out the factor γ^α will have been replaced by P^α. From Eq. (2.26) we then see that only the $\alpha = +$ term will contribute to the final answer, as P^+ is larger by far than any other component of the momentum P^α. We thus can replace γ^α with γ^+ from the start, substituting $(1/2)(k + q)^- \gamma^+ \approx (Q^2/2k^+) \gamma^+$ in to Eq. (2.34) in place of $\slashed{k} + \slashed{q}$. (We have used the fact that $\vec{q}_\perp^2 \approx Q^2$ is the largest transverse momentum, while $k^+ = x P^+ \gg q^+$.) We obtain

$$W_{\mu\nu} = \frac{1}{4m} \sum_{n,\,f} \int dk^+ \, d^2 k_\perp \, \frac{1}{S_n} \sum_{r,r''} \prod_{i=1}^{n} \frac{dx_i}{x_i} \frac{d^2 k_{i\perp}}{2(2\pi)^3}$$

$$\times \Psi_n^f \left(\{x_i, k_{i\perp}\}; \frac{k^+}{P^+}, k_\perp; r \right) \left[\Psi_n^f \left(\{x_i, k_{i\perp}\}; \frac{k^+}{P^+}, k_\perp; r'' \right) \right]^* Z_f^2$$

$$\times \bar{u}_{r''}(k) \, \gamma_\nu \gamma^+ \gamma_\mu \, u_r(k) \, \delta \left(P^+ - k^+ - \sum_{l=1}^{n} k_l^+ \right) \delta^2 \left(\vec{k}_\perp + \sum_{j=1}^{n} \vec{k}_{j\perp} \right)$$

$$\times \frac{1}{2x_{Bj} k^+} \, \delta \left(x_{Bj} - \frac{k^+}{P^+} \right), \tag{2.35}$$

where we have also made use of the last delta function in Eq. (2.34) to replace $(P^+/k^+)^2$ by $1/x_{Bj}^2$.

With the help of Table A.1 in appendix section A.1 and employing Eq. (2.35), it is easy to see that

$$W^{\mu+} = W^{+\mu} \propto \bar{u}_{r''}(k) \, \gamma^\mu \gamma^+ \gamma^+ \, u_r(k) = 0,$$

$$W^{--} \propto \bar{u}_{r''}(k) \, \gamma^- \gamma^+ \gamma^- \, u_r(k) = \bar{u}_{r''}(k) \, \gamma^- \, u_r(k) = \frac{2\delta_{r\,r''} k_\perp^2}{k^+}. \tag{2.36}$$

To find the transverse components of $W^{\mu\nu}$ we note that, from Eq. (2.14), this tensor is symmetric. Anticipating that the final result of the integrations in Eq. (2.35) yields a symmetric tensor, we can therefore symmetrize the transverse components to get

$$W^{ij} \propto \bar{u}_{r''}(k) \, \gamma^j \gamma^+ \gamma^i \, u_r(k) = \bar{u}_{r''}(k) \tfrac{1}{2} \left(\gamma^j \gamma^+ \gamma^i + \gamma^i \gamma^+ \gamma^j \right) u_r(k)$$

$$= -\tfrac{1}{2} \bar{u}_{r''}(k) \, \gamma^+ \left\{ \gamma^j, \gamma^i \right\} u_r(k) = -g^{ij} \bar{u}_{r''}(k) \, \gamma^+ u_r(k) = -g^{ij} \delta_{r\,r''} 2k^+ \tag{2.37}$$

for $i, j = 1, 2$. As $k^+ \gg k_\perp$ we see that W^{ij} is much larger than W^{--} and is, therefore, the only nonnegligible component of the hadronic tensor $W^{\mu\nu}$. (Similarly, one can show that
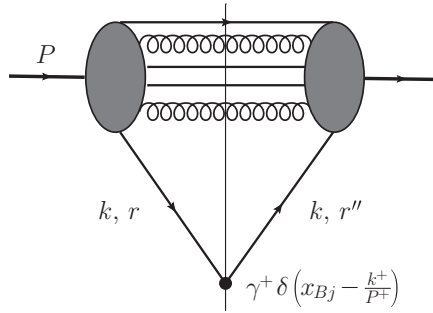
Fig. 2.6. Cut (Mueller) vertex in DIS, denoted by the solid circle.

$W^{-i} = W^{i-} \propto k_\perp^i$, which is much smaller than W^{ij} and integrates out to zero in Eq. (2.35) owing to the absence of a preferred transverse direction in the problem.)

From Eqs. (2.37) and (2.35) we see that, in the usual Feynman diagram language, the quark–photon part of the diagram in Fig. 2.3 can be replaced by a single effective vertex containing $\gamma^+ \delta(x_{Bj} - k^+/P^+)$, as shown in Fig. 2.6. This effective vertex is known as a *cut vertex* or *Mueller vertex* (Mueller 1970, 1981).

From the general decomposition of $W^{\mu\nu}$ in Eq. (2.16) and using the fact that, by our frame choice, $\vec{P}_\perp = 0$ we can write

$$W^{ij} = -W_1(x_{Bj}, Q^2)\, g^{ij} + \frac{q^i q^j}{q^2} \left[W_1(x_{Bj}, Q^2) + \frac{W_2(x_{Bj}, Q^2)}{m^2} \frac{(P \cdot q)^2}{q^2} \right]. \quad (2.38)$$

Comparing Eq. (2.38) with Eq. (2.37), for which we showed that $W^{ij} \propto g^{ij}$, we see that the hadronic tensor is given by the first term in Eq. (2.38):

$$W^{ij} = -W_1(x_{Bj}, Q^2)\, g^{ij}. \quad (2.39)$$

Substituting Eq. (2.37) into Eq. (2.35), summing over r'', and comparing the result with Eq. (2.39) we can read off the structure function W_1:

$$W_1(x_{Bj}, Q^2) = \frac{1}{4m x_{Bj}} \sum_{n,f} Z_f^2 \int dk^+ d^2 k_\perp \frac{1}{S_n} \sum_r \prod_{i=1}^n \frac{dx_i}{x_i} \frac{d^2 k_{i\perp}}{2(2\pi)^3}$$

$$\times \left| \Psi_n^f \left(\{x_i, k_{i\perp}\}; \frac{k^+}{P^+}, k_\perp; r \right) \right|^2 \delta\left(P^+ - k^+ - \sum_{l=1}^n k_l^+ \right)$$

$$\times \delta^2 \left(\vec{k}_\perp + \sum_{j=1}^n \vec{k}_{j\perp} \right) \delta\left(x_{Bj} - \frac{k^+}{P^+} \right). \quad (2.40)$$

Let us now define the *quark distribution function* by

$$q^f(x_{Bj}) = \frac{1}{2x_{Bj}} \sum_n \int d\xi \, d^2k_\perp \frac{1}{S_n} \sum_r \prod_{i=1}^n \frac{dx_i}{x_i} \frac{d^2k_{i\perp}}{2(2\pi)^3}$$

$$\times \left| \Psi_n^f \left(\{x_i, k_{i\perp}\}; \frac{k^+}{P^+}, k_\perp; r \right) \right|^2 \delta\left(1 - \xi - \sum_{l=1}^n x_l\right)$$

$$\times \delta^2\left(\vec{k}_\perp + \sum_{j=1}^n \vec{k}_{j\perp}\right) \delta\left(x_{Bj} - \xi\right), \qquad (2.41)$$

where $\xi = k^+/P^+$. With the help of Eq. (2.41) we can rewrite Eq. (2.40) as

$$W_1(x_{Bj}) = \frac{1}{2m} \sum_f Z_f^2 \, q^f(x_{Bj}). \qquad (2.42)$$

Note that both the quark distribution function and the structure function W_1 are functions of Bjorken x only! Just as in the case of DIS on a single free quark, this is Bjorken scaling.

To find the remaining structure function, W_2, we note that, as we have just shown in Eq. (2.37), $W^{ij} \propto g^{ij}$. Therefore the term in square brackets in Eq. (2.38) must be zero. Equating it to zero, and recalling the definitions of x_{Bj} and ν from Eqs. (2.2) and (2.5), we write

$$\nu \, W_2(x_{Bj}) = 2m x_{Bj} \, W_1(x_{Bj}). \qquad (2.43)$$

Using the definitions in Eqs. (2.18a) and (2.18b) we can rewrite Eq. (2.43) as

$$F_2(x_{Bj}) = 2x_{Bj} \, F_1(x_{Bj}). \qquad (2.44)$$

Equation (2.44) is known as the *Callan–Gross* relation (Callan and Gross 1969). This relation is characteristic of spin-1/2 partons, such as quarks, and would be different if the proton had constituents with a different spin interacting with the virtual photon.

Combining Eqs. (2.18a), (2.42), and the Callan–Gross relation we write

$$F_1(x_{Bj}) = \frac{1}{2} \sum_f Z_f^2 \, q^f(x_{Bj}), \qquad (2.45)$$

$$F_2(x_{Bj}) = \sum_f Z_f^2 \, x_{Bj} \, q^f(x_{Bj}). \qquad (2.46)$$

We can see that both structure functions are independent of Q^2 and are functions of x_{Bj} only. Therefore, if we assume that some nonperturbative QCD effects lead to a natural UV cutoff on the transverse momenta of the partons then the DIS cross section can be described by two functions, F_1 and F_2, that are dependent on only one variable, x_{Bj}. This is a more general form of *Bjorken scaling* (Bjorken 1969). We have now shown that Bjorken scaling results from a full parton model calculation.
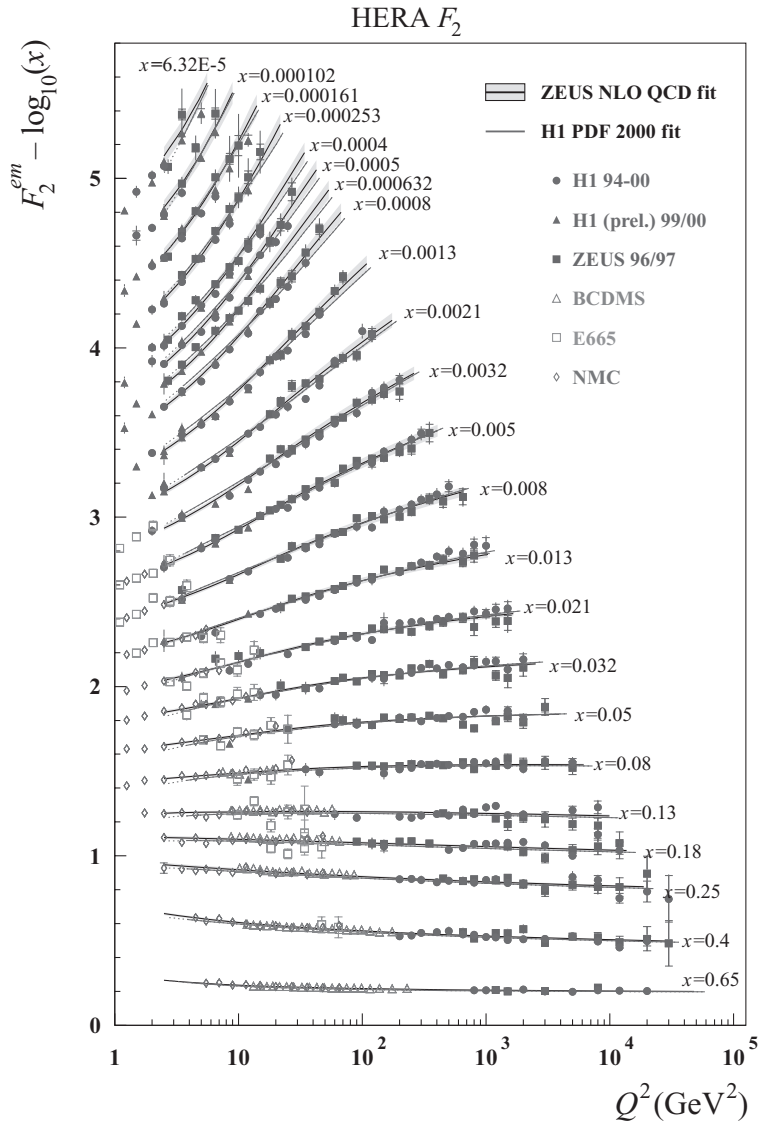
Fig. 2.7. Compilation of the world F_2 data for DIS on a proton. The proton F_2 structure function is plotted as a function of Q^2 for a range of values of x, as indicated next to the data. It can be seen that, except for very small x, F_2 is independent of Q^2, a manifestation of Bjorken scaling. (We thank Kunihiro Nagano for providing us with this figure.) A color version of this figure is available online at www.cambridge.org/9780521112574.

In Fig. 2.7 we show a summary of the world knowledge of the proton F_2 structure function. This structure function is plotted as a function of Q^2 for many different fixed values of Bjorken-x. One can clearly see that, when x is not too small, F_2 is independent of Q^2. This is the experimental manifestation of Bjorken scaling. We see that the theory we

have been presenting here agrees very well with the data, at least at the qualitative level. (The curves going through the data points result from the solution of the QCD renormalization group equations in Q^2, which are presented below.)

The quark distribution function defined in Eq. (2.41) counts the number of quarks with longitudinal momentum fraction x_{Bj}. While this may not be obvious from Eq. (2.41), we may check this statement for DIS on a single quark. Comparing Eq. (2.45) for a single flavor with Eq. (2.24) yields

$$q^f_{\text{one-quark}}(x_{Bj}) = \delta(1 - x_{Bj}) \tag{2.47}$$

meaning that our target "proton" indeed consists of a single quark which carries all the "proton" momentum, i.e., the quark is at $x_{Bj} = 1$. Equation (2.47) can also be obtained from Eq. (2.41) directly by setting $n = 0$ in the latter equation and also using $|\Psi_0^f|^2 = 1$.

As one can see from Eqs. (2.45) and (2.46), the functions F_1 and F_2 have a very simple physical meaning: namely, F_1 gives the number of partons in the hadron with longitudinal momentum fraction x_{Bj} (weighted by $Z_f^2/2$) while F_2 gives the average longitudinal momentum fraction of the partons in the hadron (weighted by Z_f^2) times the number of partons.

Using Eqs. (2.45) and (2.46) we can understand the physics behind the parton model. The proton arrives with partons in its wave function, which, for the duration of the DIS interaction, can be thought of as free particles. To be specific, let us concentrate on the F_2 structure function. The interaction of each quark with the virtual photon yields a factor $Z_f^2 x_{Bj}$, as seen in Eq. (2.46). The full expression for the proton structure function F_2 in Eq. (2.46) can be interpreted as the product of the number of quarks in the proton ($q^f(x_{Bj})$) and the amplitude for the interaction of each quark with the photon ($Z_f^2 x_{Bj}$). We thus have a clear physical picture of a proton with noninteracting partons in its wave function scattering on a virtual photon in such a way that each parton interacts with the photon independently of the other partons. We can therefore write (for the details see Sterman (1993))

$$F_2(x_{Bj}) = \sum_f \int_0^1 d\xi \, q^f(\xi) \, C_2^f \left(\frac{x_{Bj}}{\xi} \right). \tag{2.48}$$

The distribution function q^f gives the number of quarks in the proton's wave function, while the *coefficient function* C_2^f expresses the interaction between a quark with flavor f and the virtual photon. At the lowest order, considered here, $C_2^f = Z_f^2 \, \delta(x_{Bj}/\xi - 1)$. When used in Eq. (2.48) it leads to Eq. (2.46).

One can easily express the structure functions in terms of the photon–proton cross section $\sigma^{\gamma^* p}$ for transverse and longitudinal polarizations of the virtual photon. In particular one obtains (see Halzen and Martin (1984) along with the derivation in Sec. 4.1 below)

$$F_2(x_{Bj}, Q^2) = \frac{Q^2}{4\pi^2 \alpha_{EM}} \sigma^{\gamma^* p}_{tot}, \tag{2.49}$$

where $\sigma_{tot}^{\gamma^* p}$ is the total $\gamma^* p$ cross section summed over all photon polarizations. With the help of Eq. (2.49), Eq. (2.48) can be rewritten directly for the cross section as

$$\sigma_{tot}^{\gamma^* p}(x_{Bj}, Q^2) = \sum_f \int \frac{d\xi}{\xi}\, \xi\, q^f(\xi)\, \hat{\sigma}^{\gamma^* + \text{parton} f}\left(\frac{x_{Bj}}{\xi}, Q^2\right)$$

$$= \sum_f \int dy'\, N^f(y')\, \hat{\sigma}^{\gamma^* + \text{parton} f}\left(e^{-(y-y')}, Q^2\right), \qquad (2.50)$$

where $N^f(y = \ln 1/x_{Bj}) = x_{Bj}\, q^f(x_{Bj})$ is the number of partons (quarks) inside the hadron having flavor f per unit *rapidity* $y = \ln(P^+/k^+) = \ln 1/x_{Bj}$. The factor $\hat{\sigma}^{\gamma^* + \text{parton} f}(x, Q^2)$ is the cross section for parton–virtual photon scattering. In Eq. (2.50) we have $y = \ln 1/x_{Bj}$ and $y' = \ln 1/\xi$. One can see from Eq. (2.25) that in the "naive" parton model considered here one has

$$\hat{\sigma}^{\gamma^* + \text{parton} f}(x_{Bj}, Q^2) = \frac{4\pi^2 \alpha_{EM}}{Q^2} Z_f^2\, x_{Bj}\, \delta(1 - x_{Bj}) = \frac{4\pi^2 \alpha_{EM}}{Q^2} Z_f^2\, \delta(y). \qquad (2.51)$$

Using Eq. (2.51) in Eq. (2.50) reduces the latter to Eq. (2.46).

Equations (2.48) and (2.50) show that, in the framework of the parton approach, finding cross sections is reduced to two separate problems: finding the light cone wave function of the hadron, which does not depend on the probe, and calculating the cross section for scattering of the parton on the probe, γ^* in the case of electron DIS. The process is illustrated in Fig. 2.10. This simple parton model with an additional obvious assumption that the partons are quarks, anti-quarks, and gluons is able to describe a striking amount of experimental data. See Feynman (1972), as well as our main textbooks Peskin and Schroeder (1995) and Halzen and Martin (1984), for more detailed comparisons of the parton model with the data.

2.3 Space–time structure of DIS processes

Equation (2.48) is very simple and intuitively sound. It would be useful to visualize it in terms of the space–time dynamics of partons. For this purpose we will rewrite Eq. (2.14) for the cross section of the virtual photon interaction as the imaginary part of the Compton scattering amplitude at zero angle. In the space–time representation it looks as follows:

$$W_{\mu\nu}(x_{Bj}, Q^2) = \frac{1}{2\pi m} \text{Im}\left\{ i \int d^4x\, e^{iq\cdot x} \langle P|\text{T}\,[J_\mu(x)\, J_\nu(0)]|P\rangle \right\}, \qquad (2.52)$$

where as usual $|P\rangle$ denotes the state of the target (the proton) and T denotes time-ordering. The right-hand side of Eq. (2.52) is simply the imaginary part of the forward scattering amplitude for the photon–proton interaction. The coordinate four-vector x^μ in the forward amplitude describes the space–time separation between absorption and re-emission of the virtual photon by a quark inside the proton.

Let us first work in the rest frame of the proton. Just as in Sec. 2.1 we have $P^\mu = (m, \vec{0})$. However, now we are interested in the photon–proton interaction: we can forget about the

electron in Sec. 2.1 that gave rise to the photon and choose our coordinate axis in such a way that the photon's four-momentum is $q^\mu = (q^0, \vec{0}_\perp, q^3)$. We then have $2P \cdot q = 2q^0 m = Q^2/x_{Bj}$, so that

$$q^0 = \frac{Q^2}{2mx_{Bj}} \gg Q \tag{2.53}$$

since $Q \gg m$ and $x_{Bj} \le 1$. By the definition of Q^2 we have $0 \le Q^2 = -q^2 = (q^3)^2 - (q^0)^2$. Hence $q^3 \ge q^0 \gg Q$. Therefore $q^0 \approx q^3 \gg Q$. We can then write

$$q^+ = q^0 + q^3 \approx 2q^0,$$

$$q^- = q^0 - q^3 = \frac{q^+ q^-}{q^+} \approx -\frac{Q^2}{2q^0} = -mx_{Bj}. \tag{2.54}$$

Writing $q \cdot x$ in the exponent in Eq. (2.52) as $\frac{1}{2}(q^+ x^- + q^- x^+)$, we argue that the typical x^- range is given by $2/q^+$, while the typical x^+ range is given by $2/q^-$. Therefore

$$x^- \approx \frac{2}{q^+} \approx \frac{2mx_{Bj}}{Q^2} \ll \frac{1}{\mu},$$

$$x^+ \approx \frac{2}{|q^-|} \approx \frac{2}{mx_{Bj}} \ge \frac{1}{\mu}, \tag{2.55}$$

where $\mu \sim \Lambda_{QCD} \sim m$ is the scale of the nonperturbative (soft) QCD interactions, which gives the average transverse momenta of the partons in the parton model. From Eq. (2.55) we see that, for large Q, one has $x^- = t - z \approx 0$ and $x^+ = t + z \approx 2t \approx 2/(mx_{Bj})$. Therefore the light cone time of observation is given by

$$x^+ \approx \frac{2}{mx_{Bj}}. \tag{2.56}$$

This time is known as the *Ioffe time* (Ioffe 1969, Gribov, Ioffe, and Pomeranchuk 1966). It can be interpreted as the typical longitudinal distance of the interaction (the coherence length). We see that this longitudinal range in DIS increases with decreasing Bjorken x.[3]

We can also determine the transverse coordinate resolution of the virtual photon in DIS. Imposing the causality of the interactions in the forward scattering amplitude (2.52), i.e., $x^2 = x^+ x^- - x_\perp^2 > 0$, and using Eq. (2.55) we get

$$x_\perp^2 < x^+ x^- \propto \frac{4}{Q^2} \ll \frac{1}{\mu^2}. \tag{2.57}$$

We see that the typical transverse resolution of the virtual photon is of order $1/Q$. Therefore the photon can resolve very short distances, deep inside the proton: this enables it to "pick out" a quark with which to interact independently of the other "spectator" partons. This

---

[3] The careful reader will notice that for small enough x_{Bj} the light cone time, i.e., the coherence length, in Eq. (2.56) becomes larger than the size of the target proton. Therefore at least one of the electromagnetic currents J_μ in Eq. (2.52) has to be located outside the proton. How can an interaction with the proton happen outside the proton? We will explain this phenomenon in more detail later, in Chapter 4, but here we briefly note that at very small x_{Bj} the incoming current can decay into a quark–antiquark pair outside the proton, the $q\bar{q}$ pair subsequently interacting with the proton.
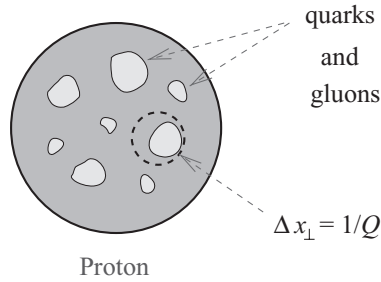
Fig. 2.8. A depiction of a proton during DIS in the transverse plane. The blobs represent partons (quarks and gluons), while the dashed circle denotes the virtual photon. A color version of this figure is available online at www.cambridge.org/9780521112574.

conclusion is illustrated in Fig. 2.8, where we show a proton in the transverse plane with the quarks and gluons in its wave function denoted by blobs with random shapes. The virtual photon is represented by a dashed circle whose size is of order $1/Q$, in agreement with Eq. (2.57). One can see explicitly now that the DIS experiment works as a microscope: varying Q^2 changes the transverse size of the photon and so changes the "resolution" of the DIS experiment, allowing the virtual photon to interact with partons of different transverse extent.

Now, let us consider DIS process in the IMF or Bjorken frame. There the proton momentum is given by Eq. (2.19) (or, equivalently, Eq. (2.26)), while the virtual photon momentum is given by Eq. (2.20) (Eq. (2.28)). We see that $2P \cdot q \approx 2Pq^0 = Q^2/x_{Bj}$, giving

$$q^0 \approx \frac{Q^2}{2x_{Bj}P}. \tag{2.58}$$

We conclude that the interaction time in the IMF is

$$t_{DIS} \approx \frac{1}{q^0} \approx \frac{2x_{Bj}P}{Q^2}. \tag{2.59}$$

This time needs to be compared with the typical time scale with which partons interact inside the proton. In the rest frame of the proton, the interparton interaction time is nonperturbatively long, of order $1/\mu$. In the IMF or Bjorken frame the time is dilated by the boost factor P/m, giving

$$t_{partons} \approx \frac{1}{\mu} \frac{P}{m}. \tag{2.60}$$

Comparing Eqs. (2.59) and (2.60) one can see clearly that since $x_{Bj}\mu m \le \mu m \ll Q^2$ we have
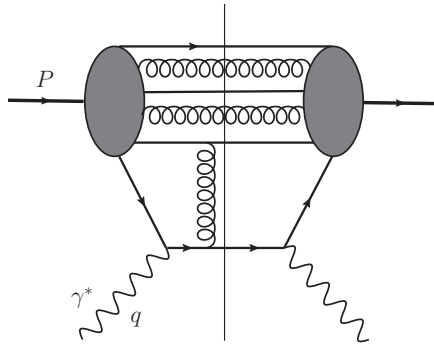
$$t_{DIS} \ll t_{partons}. \tag{2.61}$$

Fig. 2.9. An example of a higher-twist correction.

Therefore we have justified a main assumption in Sec. 2.2, that the typical time scale of interpartonic interactions is much longer than the typical time scale of DIS. One does not have to worry about partons interacting with each other during DIS.

The time-scale argument presented here can be supported by explicit diagrammatic calculations showing that diagrams in which the quark struck by the photon exchanges gluons with other partons, such as the graph shown in Fig. 2.9, are suppressed by powers of μ^2/Q^2 and m^2/Q^2. Such corrections are known as *higher-twist terms*. The twist of an operator is defined as its mass dimension minus its spin (Peskin and Schroeder 1995, Sterman 1993). In the operator product expansion (OPE) for the hadronic tensor $W^{\mu\nu}$ in Eq. (2.14) the contribution of higher-twist operators enters with an extra $1/Q^2$ suppression compared with the leading large-Q^2 term that we found above. In the language of LCPT the higher-twist operators correspond to a proton light cone wave function in which we tag on (i.e., detect) more than one particle. The reader particularly interested in twist expansions is referred to Sterman (1993) or Peskin and Schroeder (1995).

The transverse space dynamics is particularly simple in the IMF/Bjorken frame: from Eq. (2.58) we see that $q^0 \ll Q$, so that $Q^2 = q_\perp^2 - (q^0)^2 \approx q_\perp^2$. Hence the transverse resolution of the virtual photon is

$$x_\perp \approx \frac{1}{q_\perp} \approx \frac{1}{Q}, \tag{2.62}$$

just as in the proton's rest frame.

Equation (2.55) also has a very clear meaning in another frame, the Breit frame, where the photon momentum is equal to

$$q^\mu = (q^0 = 0, \vec{0}_\perp, q^3 = -Q) \tag{2.63}$$

and the proton's momentum is given by Eq. (2.26), as it is in the IMF. In this frame $q^+ = -q^- = -Q$; thus $x^- \propto 1/Q$ and $x^+ \propto 1/Q$, leading to $x_\perp^2 < 1/Q^2$ by a causality argument just as in the proton's rest frame. All space and time intervals between photon absorption and re-emission are short, of order $1/Q$. The photon interacts with the target during a very short time interval. The interparton interaction time in the Breit frame is the
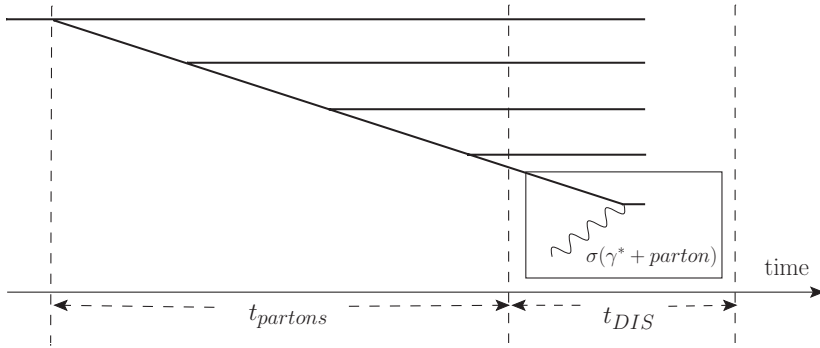
Fig. 2.10. The space–time structure of DIS in the IMF/Bjorken and Breit frames. For this illustration, it is sufficient that all partons (both quarks and gluons) are denoted by straight solid lines, for simplicity.

same as in the IMF/Bjorken frame and is given by Eq. (2.60). Then one can easily see that, with $t_{DIS} = 1/Q$ in the Breit frame and since $PQ \gg \mu m$, we still have $t_{partons} \gg t_{DIS}$ in this frame.

Having these estimates in mind we can view the deep inelastic scattering process in either the Breit or the IMF/Bjorken frame, as shown in Fig. 2.10. The fast-moving particle (the proton), long before the interaction, "produces" a system of point-like particles (partons) which can be described by a light cone wave function. At the moment of interaction, the parton with the lowest energy (the "wee" parton) interacts with the virtual photon. The virtual photon in the Breit frame is a standing wave that interacts only with partons that have the same wavelength; in other words, it interacts with the parton whose momentum is equal to Q/2. The last statement follows from momentum conservation for the wee parton, whose momentum is k before and k' after its interaction with photon, namely,

$$k^0 = k'^0, \quad k^3 - k'^3 = Q, \quad \vec{k}_\perp = \vec{k}'_\perp. \tag{2.64}$$

(To obtain Eq. (2.64) note that $k' = k + q$ and use Eq. (2.63).) From Eq. (2.64), and assuming that the incoming parton is on mass shell, one can show that $k^3 = -k'^3 = Q/2$. Assuming also that $Q \gg k_\perp$ and neglecting the quark mass we get $k^0 \approx k^3 = Q/2$, leading to $k^+ \approx Q$. The fraction of the proton's light cone momentum P^+ carried by the struck quark is equal to $x = k^+/P^+ \approx Q/P^+ = Q^2/(P^+q^-) = x_{Bj}$, just as in Eq. (2.33).

Therefore the DIS process happens in two stages. The first stage is the creation of many point-like partons and can be described by the light cone wave function of the fast-moving hadron. The second stage is the interaction of the slowest (wee) parton with the virtual photon, which occurs at low energies. It should be stressed that in this section we have not used the fact that the transverse momenta of partons are restricted in the UV, though we did in the previous section. This fact gives us hope that the whole structure, consisting of the wave function of the fast-moving hadron and the interaction of the parton with the photon, will remain correct in a more general approach. However, the wee parton interaction could be more complicated than in the naive parton model.

2.4 Violation of Bjorken scaling;
the Dokshitzer–Gribov–Lipatov–Altarelli–Parisi evolution equation

2.4.1 Parton distributions

Let us study the QCD corrections to the naive parton model presented above. First we rewrite the quark distribution function $q^f(x, Q^2)$ for a quark of flavor f from Eq. (2.41) as follows:

$$q^f(x, Q^2) = \sum_n \frac{1}{x} \int \frac{d^2k_\perp}{2(2\pi)^3} \frac{1}{S_n} \sum_{\sigma=\pm 1} \prod_{i=1}^{n} \frac{dx_i}{x_i} \frac{d^2k_{i\perp}}{2(2\pi)^3}$$
$$\times |\Psi_n^f(\{x_i, k_{i\perp}\}; x, k_\perp; \sigma)|^2 (2\pi)^3$$
$$\times \delta^2\left(\vec{k}_\perp + \sum_{j=1}^{n} \vec{k}_{j\perp}\right) \delta\left(1 - x - \sum_{l=1}^{n} x_l\right). \tag{2.65}$$

The quark carries a fraction x of the longitudinal momentum of the proton; x is identical to the Bjorken-x variable defined in Eq. (2.2). Unlike in the naive parton model the quark distribution function now depends on the momentum scale Q^2, which enters Eq. (2.65) as the renormalization scale. Roughly, this implies that the integral over the quark's transverse momentum $k_\perp$ is bounded from above by Q, so that $k_\perp \leq Q$. The same applies to the other transverse momentum integrals in (2.65) along with the virtual loop integrals within the wave function Ψ_n. (In the naive parton model, we assumed that the $k_\perp$-integrals were sufficiently convergent that one could simply replace Q in the upper limit of integration by infinity without changing the value of the integral; this is, strictly speaking, only true for super-renormalizable theories and so is not true for QCD.) The goal of this subsection is to understand this Q-dependence in more detail.

The light cone wave function $\Psi_n^f(\{x_i, k_{i\perp}\}; x, k_\perp; \sigma)$ describes a Fock state in the proton containing the quark we are measuring along with n "spectator" partons with transverse momenta $k_{i\perp}$ and longitudinal momentum fractions x_i. The sum over n runs from some small number, determined by the nonperturbative physics defining the proton, up to ∞. (If we were studying the wave function of a single quark under the assumption that it is completely perturbative, then n would run from 0 to ∞.) Note that the quark helicity, which was labeled r in Sec. 2.2 to avoid confusion with the proton polarization, will be labeled from now on by σ, since here the proton helicity does not enter our calculations explicitly.

The quark distribution function (2.65) is illustrated by the diagram in Fig. 2.11. The definition (2.65) is the LCPT analogue of the standard operator definition in the light cone gauge $A^+ = 0$ (see for instance Sterman (1993)).

In analogy with (2.65) we can define the gluon distribution function:

$$G(x, Q^2) = \sum_n \frac{1}{x} \int \frac{d^2k_\perp}{2(2\pi)^3} \frac{1}{S_n} \sum_{\lambda=\pm 1} \prod_{i=1}^{n} \frac{dx_i}{x_i} \frac{d^2k_{i\perp}}{2(2\pi)^3}$$
$$\times |\Psi_n(\{x_i, k_{i\perp}\}; x, k_\perp; \lambda)|^2$$
$$\times (2\pi)^3 \delta^2\left(\vec{k}_\perp + \sum_{j=1}^{n} \vec{k}_{j\perp}\right) \delta\left(1 - x - \sum_{l=1}^{n} x_l\right). \tag{2.66}$$
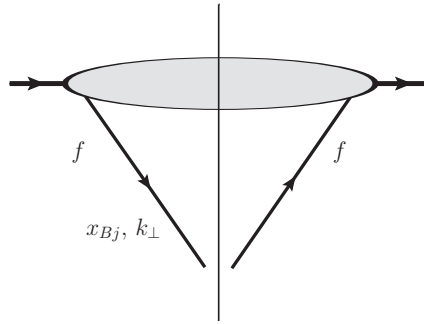
Fig. 2.11. A diagrammatic representation of the quark distribution function. The vertical solid line separates the light cone wave function from its complex conjugate.
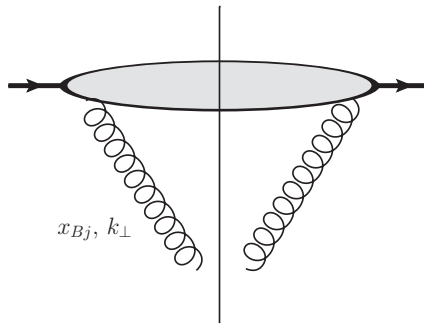

Fig. 2.12. A diagrammatic representation of the gluon distribution function.

Here $\Psi_n(\{x_i, k_{i\perp}\}; x, k_\perp; \lambda)$ is the proton light cone wave function containing n "specta-tors" along with a measured *gluon* having longitudinal momentum fraction x, transverse momentum $k_\perp$, and polarization λ. Again Q^2 enters (2.66) as the renormalization scale. The definition of the gluon distribution function given by Eq. (2.66) is the LCPT analogue of the operator definition in terms of gluon operators in the light cone gauge $A^+ = 0$ (Sterman 1993). It is illustrated in Fig. 2.12.

The $k_\perp$-integral in the definition of $q^f(x, Q^2)$ given in Eq. (2.65) is effectively cut off by Q, making the quark distribution function Q-dependent in general. The essential idea of Bjorken scaling is that for very large Q we can simply set the upper cutoff of the $k_\perp$-integral to infinity. In the naive parton model it is assumed that the $k_\perp$-integral is convergent in the UV, owing to some (presumed nonperturbative) universal cutoff. The resulting quark distribution becomes a function of x only, $q^f(x, Q^2 \to \infty) \approx q^f(x)$. This leads to the Bjorken scaling seen in Eqs. (2.45) and (2.46).

In reality the $k_\perp$-integral in Eq. (2.65) (and that in Eq. (2.66)) is not convergent in the UV and so needs this Q^2 cutoff: hence a Q^2-dependence remains in the quark and gluon distributions even at very high Q^2. To determine the Q^2-dependence of the distribution functions one needs to understand exactly how the proton's light cone wave function Ψ_n
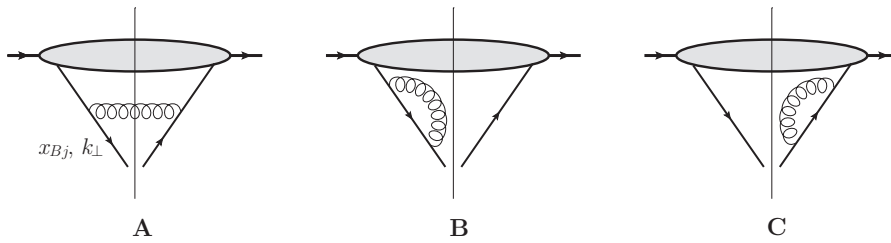
Fig. 2.13. Lowest-order QCD corrections to the quark distribution function. The virtual diagrams should be understood as including instantaneous terms.

depends on $k_\perp$. To do so we have to assume that at least part of the distribution function is perturbative. In terms of diagrams this perturbative dynamics takes place in the part of the diagram adjacent to the parton that we are describing by the distribution function. This will be justified later by the large transverse momentum of the parton. We thus need to calculate the QCD corrections to the parton distribution functions of the naive parton model pictured in Figs. 2.11 and 2.12.

2.4.2 Evolution for quark distribution

Let us start with the quark distribution function $q^f(x, Q^2)$ shown in Fig. 2.11. The lowest-order QCD corrections to $|\Psi_n^f(\{x_i, k_{i\perp}\}; x, k_\perp; \sigma)|^2$ are shown in Fig. 2.13. They consist of the "real" emission diagram A and the "virtual" diagrams B and C. (The virtual corrections in LCPT should include graphs with instantaneous terms; these are not shown explicitly.) Diagrams in which the gluon line attaches to other partons in the wave function denoted by the oval (i.e., diagrams with the gluon going into the oval) are suppressed. To see why this is so, one has to identify the resummation parameter of the calculation to be performed shortly. Indeed each diagram in Fig. 2.13 has an extra factor equal to the coupling α_s as compared with the naive parton model quark distribution in Fig. 2.11. However, we will not calculate the rest of the diagram exactly: instead we will extract the leading contribution at large Q^2. These leading contributions, after integration over $k_\perp$, will turn out to be proportional to $\ln(Q^2/\Lambda_{QCD}^2)$. Hence the diagrams in Fig. 2.13 will each give us an expression proportional to $\alpha_s \ln(Q^2/\Lambda_{QCD}^2)$. This will be the resummation parameter of our approximation: for each power of α_s we will pick up one power of $\ln(Q^2/\Lambda_{QCD}^2)$. Owing to asymptotic freedom at large Q^2 we have $\alpha_s(Q^2) \ll 1$ while $\ln(Q^2/\Lambda_{QCD}^2) \gg 1$. Our resummation parameter is thus the product of a small quantity (the coupling) and a large quantity (the logarithm), and therefore

$$\alpha_s \ln \frac{Q^2}{\Lambda_{QCD}^2} \sim 1. \tag{2.67}$$

The resummation of the parameter in Eq. (2.67) is called the leading logarithmic approximation (LLA).
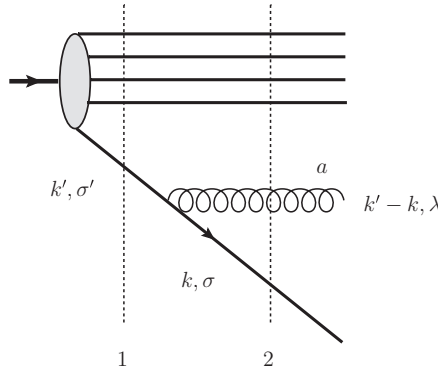
Fig. 2.14. Lowest-order correction to the proton light cone wave function contributing to the quark distribution. The vertical dotted lines denote intermediate states.

As one can show explicitly using the techniques we will develop below, the diagrams with an extra gluon connecting to the oval are, in fact, outside the leading logarithmic approximation. That is, they would generate powers of the coupling α_s not enhanced by powers of the logarithm of Q^2. This is why such diagrams are neglected in our analysis.

We will begin by calculating the diagram in Fig. 2.13A. Instead of calculating the diagram for the wave function squared it is better to start by calculating corrections to the wave function itself. The correction to the light cone wave function corresponding to Fig. 2.13A is shown in Fig. 2.14. There the intermediate states are denoted by the dotted vertical lines and are labeled 1 and 2.

Denoting by $\Psi^f_{n-1}(\{x_i, k_{i\perp}\}; x', k'_\perp; \sigma')$ the wave function for a proton with $n-1$ spectator partons (i.e., without the gluon emitted in Fig. 2.14), we note that the energy denominator corresponding to intermediate state 1 (denoted by the left-hand vertical dotted line) is already included in Ψ_{n-1}. Using the rules of LCPT outlined in Sec. 1.3 and their modification for the calculation of wave functions in Sec. 1.4, we can write down the contribution to the proton's wave function from the diagram in Fig. 2.14 as

$$\Psi^f_n\left(\{k^+_i, k_{i\perp}\}; x, k_\perp; \sigma\right) = \frac{g t^a\, \theta(k^+)\, \theta(k'^+ - k^+)}{(k' - k)^- + k^- + \sum_{j=1}^{n-1} k^-_j - P^-}$$

$$\times\; \frac{\bar{u}_\sigma(k)\, \gamma \cdot \epsilon^*_\lambda(k' - k)\, u_{\sigma'}(k')}{k'^+}\; \Psi^f_{n-1}\left(\{k^+_i, k_{i\perp}\}; x', k'_\perp; \sigma'\right). \qquad (2.68)$$

Here g is the QCD coupling, t^a is the color matrix (the gluon carries color a), and $x' = k'^+/P^+$. The quark line carrying momentum k' is internal and therefore contributes a factor $1/k'^+$ which is not included in the definition of the light cone wave function Ψ^f_{n-1} and so has to be included explicitly in Eq. (2.68). The intermediate state 2 from Fig. 2.14 gives the

light cone energy denominator in Eq. (2.68):

$$\frac{1}{(k'-k)^- + k^- + \sum_{j=1}^{n-1} k_j^- - P^-} \equiv \frac{1}{\frac{(\vec{k}'_\perp - \vec{k}_\perp)^2}{k'^+ - k^+} + \frac{\vec{k}_\perp^2}{k^+} + \sum_{j=1}^{n-1} \frac{\vec{k}_j^2}{k_j^+} - P^-}. \tag{2.69}$$

Here P^- is the light cone energy of the incoming proton state. It is negligibly small, as it is inversely proportional to the large light cone plus momentum of the proton, $P^- \sim 1/P^+$, not enhanced by a large transverse momentum. (Indeed, for a "proton" consisting of a single valence quark of mass m_q one has $P^- = (\vec{P}_\perp^2 + m_q^2)/P^+$ with $\vec{P}_\perp$ the transverse momentum of the "proton".)

We are working in the $A^+ = 0$ light cone gauge. The gluon polarization vector is

$$\epsilon_\lambda^\mu(k'-k) = \left(0, \frac{2\vec{\epsilon}_\perp^\lambda \cdot k'^+ - k^+}{\vec{k}'_\perp - \vec{k}_\perp}, \vec{\epsilon}_\perp^\lambda\right)$$

in the $(+,-,\perp)$ notation with $\vec{\epsilon}_\perp^\lambda = -(1/\sqrt{2})(\lambda, i)$. One can thus write

$$\bar{u}_\sigma(k)\, \gamma \cdot \epsilon_\lambda^*(k'-k)\, u_{\sigma'}(k') = \bar{u}_\sigma(k)\, \gamma^+ u_{\sigma'}(k')\, \frac{\vec{\epsilon}_\perp^{\lambda*} \cdot (\vec{k}'_\perp - \vec{k}_\perp)}{k'^+ - k^+}$$
$$- \bar{u}_\sigma(k)\, \vec{\gamma}_\perp\, u_{\sigma'}(k') \cdot \vec{\epsilon}_\perp^{\lambda*}. \tag{2.70}$$

Using the tables for Dirac matrix elements from appendix section A.1 one obtains after some algebra

$$\bar{u}_\sigma(k)\, \gamma \cdot \epsilon_\lambda^*(k'-k)\, u_{\sigma'}(k') = -\frac{\delta_{\sigma\sigma'}}{\sqrt{z}\,(1-z)}\, \vec{\epsilon}_\perp^{\lambda*} \cdot (\vec{k}_\perp - z\,\vec{k}'_\perp)$$
$$\times\, [1 + z + \sigma\lambda(1-z)], \tag{2.71}$$

where $z = k^+/k'^+$ and we have assumed that the quarks are massless for simplicity. In arriving at Eq. (2.71) we have used $\vec{\epsilon}_\perp^{\lambda*} \times \vec{k}_\perp = i\lambda\, \vec{\epsilon}_\perp^{\lambda*} \cdot \vec{k}_\perp$, which is valid in two dimensions.

We will be working in the approximation where all transverse momenta are ordered:

$$Q^2 \gg k_\perp^2 \gg k'^2_\perp \gg k_{n-1,\perp}^2 \gg \cdots \gg k_{1,\perp}^2 \sim \Lambda_{QCD}^2. \tag{2.72}$$

Such a regime corresponds to the LLA discussed above. One also assumes that all relevant large transverse momentum scales are much larger than the quark masses, which justifies the massless quark approximation we have just used. In the regime defined by Eq. (2.72) the light cone energy denominator becomes (see Eq. (2.69))

$$\frac{1}{(k'-k)^- + k^- + \sum_{j=1}^{n-1} k_j^- - P^-} \approx \frac{k'^+ z(1-z)}{\vec{k}_\perp^2}. \tag{2.73}$$

Substituting Eqs. (2.71) and (2.73) into Eq. (2.68) and assuming that $k_\perp^2 \gg k_\perp'^2$ yields

$$
\Psi_n^f(\{x_i, k_{i\perp}\}; x, k_\perp; \sigma) = -g t^a \, \theta(z) \, \theta(1-z) \, \delta_{\sigma\sigma'} \, \sqrt{z} \, \frac{\vec{\epsilon}_\perp^{\lambda *} \cdot \vec{k}_\perp}{k_\perp^2}
$$

$$
\times \, [1 + z + \sigma\lambda(1-z)] \, \Psi_{n-1}^f\left(\{x_i, k_{i\perp}\}; x', k_\perp'; \sigma'\right). \quad (2.74)
$$

Multiplying the wave function (2.74) by its complex conjugate and summing over the quark and gluon polarizations and colors we get

$$
\sum_{\sigma, \sigma', \lambda, a} |\Psi_n^f(\{x_i, k_{i\perp}\}; x, k_\perp; \sigma)|^2 = 8\pi\alpha_s \, C_F \, \theta(z) \, \theta(1-z) \, z(1+z^2) \, \frac{1}{k_\perp^2}
$$

$$
\times \sum_{\sigma'=\pm 1} |\Psi_{n-1}^f\left(\{x_i, k_{i\perp}\}; x', k_\perp'; \sigma'\right)|^2; \quad (2.75)
$$

in arriving at Eq. (2.75) we have used the fact that $\vec{\epsilon}_\perp^\lambda = -(1/\sqrt{2})(\lambda, i)$ and $\sum_{a=1}^{N_c^2-1} t^a \, t^a = C_F$, where

$$
C_F = \frac{N_c^2 - 1}{2N_c} \quad (2.76)
$$

is the Casimir operator in the fundamental representation of SU(N_c).

Substituting Eq. (2.75) into the definition of the quark distribution function (2.65) yields the contribution of the diagram in Fig. 2.13A:

$$
q_A^f(x, Q^2) = \sum_n \frac{1}{x} \int \prod_{i=1}^{n-1} \frac{dx_i}{x_i} \frac{d^2 k_{i\perp}}{2(2\pi)^3} \frac{d^2 k_\perp}{2(2\pi)^3} \frac{d(k'^+ - k^+)}{k'^+ - k^+} \frac{d^2(\vec{k}_\perp' - \vec{k}_\perp)}{2(2\pi)^3}
$$

$$
\times \, 8\pi\alpha_s C_F \, \theta(z) \, \theta(1-z) \, \frac{z(1+z^2)}{k_\perp^2} \sum_{\sigma'=\pm 1} |\Psi_{n-1}^f\left(\{x_i, k_{i\perp}\}; x', k_\perp'; \sigma'\right)|^2
$$

$$
\times \, (2\pi)^3 \, \delta^2\left(\vec{k}_\perp' + \sum_{j=1}^{n-1} \vec{k}_{j\perp}\right) \delta\left(1 - x' - \sum_{l=1}^{n-1} x_l\right). \quad (2.77)
$$

Note that the symmetry factor S_n from Eq. (2.65) is eliminated by the momentum ordering (2.72), which makes the particles in the wave function distinct. Since we are keeping k^+ fixed, the integral over $k'^+ - k^+$ can be rewritten as follows:

$$
\int_0^{P^+ - k^+} \frac{d(k'^+ - k^+)}{k'^+ - k^+} = \int_{k^+}^{P^+} \frac{dk'^+}{k'^+ - k^+} = \int_x^1 \frac{dz}{z(1-z)}. \quad (2.78)
$$

Then we can rewrite Eq. (2.77):

$$q_A^f(x, Q^2) = \frac{\alpha_s\, C_F}{2\pi}\, \frac{1}{x} \int\limits^{Q^2} \frac{dk_\perp^2}{k_\perp^2} \int\limits_x^1 dz\, \frac{1+z^2}{1-z}$$

$$\times \sum_n \int \prod_{i=1}^{n-1} \frac{dx_i}{x_i}\, \frac{d^2 k_{i\perp}}{2(2\pi)^3}\, \frac{d^2 k'_\perp}{2(2\pi)^3} \sum_{\sigma'=\pm 1} |\Psi_{n-1}^f\left(\{x_i, k_{i\perp}\}; x', k'_\perp; \sigma'\right)|^2$$

$$\times (2\pi)^3\, \delta^2\left(\vec{k}'_\perp + \sum_{j=1}^{n-1} \vec{k}_{j\perp}\right) \delta\left(1 - x' - \sum_{l=1}^{n-1} x_l\right), \tag{2.79}$$

where the integral over $k'_\perp$ is cut off by $k_\perp$ from above owing to our momentum ordering $Q^2 \gg k_\perp^2 \gg k_\perp'^2 \gg \Lambda_{QCD}^2$.

Comparing with Eq. (2.65) we recognize the last two lines of Eq. (2.79) as $x'q^f(x', k_\perp^2)$. Equation (2.79) thus gives

$$q_A^f(x, Q^2) = \frac{\alpha_s\, C_F}{2\pi}\, \frac{1}{x} \int\limits^{Q^2} \frac{dk_\perp^2}{k_\perp^2} \int\limits_x^1 dz\, \frac{1+z^2}{1-z}\, x'q^f(x', k_\perp^2). \tag{2.80}$$

Remembering that $z = k^+/k'^+ = x/x'$, we write

$$q_A^f(x, Q^2) = \frac{\alpha_s\, C_F}{2\pi} \int\limits^{Q^2} \frac{dk_\perp^2}{k_\perp^2} \int\limits_x^1 \frac{dz}{z}\, \frac{1+z^2}{1-z}\, q^f\left(\frac{x}{z}, k_\perp^2\right). \tag{2.81}$$

This is the contribution of diagram A in Fig. 2.13 to the quark distribution function. As promised above, it contains the coupling α_s as a factor and a logarithmic integral $dk_\perp^2/k_\perp^2$ cut off by Q^2 in the UV and by some nonperturbative scale $\sim \Lambda_{QCD}^2$ in the infrared (IR). We have thus shown that the leading large-Q^2 contribution of diagram A in Fig. 2.13 to the quark distribution function is proportional to $\alpha_s \ln Q^2/\Lambda_{QCD}^2$.

Now imagine that we slowly increase Q^2. As Q^2 gets larger, the phase space for the emitted gluons increases, generating larger and larger $\ln(Q^2/\Lambda_{QCD}^2)$ values and thus increasing the probability of gluon emission. The modification $\delta q_A^f(x, Q^2)$ of the quark distribution with increasing Q^2 due to the gluon emission in Fig. 2.13A can be obtained by differentiating Eq. (2.81) with respect to Q^2:

$$Q^2\, \frac{\partial q_A^f(x, Q^2)}{\partial Q^2} = \frac{\alpha_s\, C_F}{2\pi} \int\limits_x^1 \frac{dz}{z}\, \frac{1+z^2}{1-z}\, q^f\left(\frac{x}{z}, Q^2\right). \tag{2.82}$$

An example of a diagram that does not give a leading logarithmic contribution is shown in Fig. 2.15, where the oval of Fig. 2.13 is reduced to a gluon line for simplicity. The dotted vertical lines in Fig. 2.15 represent the intermediate states contributing light cone energy denominators. The diagram is of order α_s^2. Let us show that it does not give an LLA contribution, by using the results obtained above. We will work in the transverse
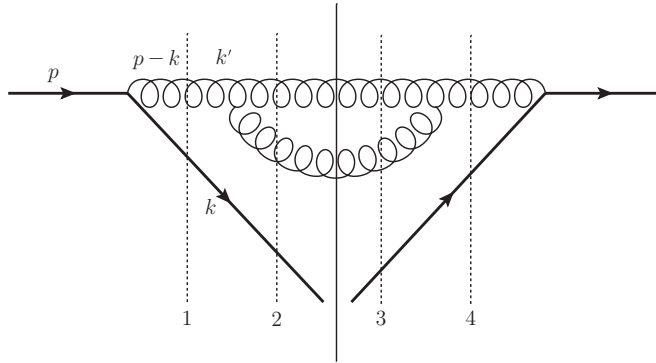
Fig. 2.15. An example of a diagram outside the leading-logarithmic approximation.

momentum ordering approximation of Eq. (2.72): $k_\perp^2 \gg k_\perp'^2$ in terms of the momentum labeling in Fig. 2.15. Keeping track of the transverse momenta we see that the energy denominators of the intermediate states 1 through 4 in Fig. 2.15 each give $1/k_\perp^2$, since they are dominated by the large light cone energy of the k-quark line (cf. Eq. (2.73)). In the same large-$k_\perp$ approximation each quark–gluon splitting gives a factor $\vec{k}_\perp$ in the amplitude (cf. Eq. (2.71)) for the net contribution of $k_\perp^2$. Assuming that gluon–gluon splitting gives a similar factor $k_\perp^2$ (this will be demonstrated explicitly in Sec. 2.4.4 below), we conclude that the contribution of the graph in Fig. 2.15 is proportional to $(1/k_\perp^2)^4 (k_\perp^2)^2 = 1/k_\perp^4$. Performing the integrals over $k_\perp^2$ and $k_\perp'^2$ with the $k_\perp^2 \gg k_\perp'^2 \gg \Lambda_{QCD}^2$ ordering, we find that the diagram in Fig. 2.15 is proportional to

$$\alpha_s^2 \int_{\Lambda_{QCD}^2}^{Q^2} dk_\perp^2 \int_{\Lambda_{QCD}^2}^{k_\perp^2} \frac{dk_\perp'^2}{k_\perp^4} \approx \alpha_s^2 \int_{\Lambda_{QCD}^2}^{Q^2} \frac{dk_\perp^2}{k_\perp^2} = \alpha_s^2 \ln \frac{Q^2}{\Lambda_{QCD}^2}. \qquad (2.83)$$

We observe that this diagram is certainly beyond the LLA, as it brings in two powers of α_s with only one power of $\ln(Q^2/\Lambda_{QCD}^2)$, whereas an LLA diagram at the same order in α_s would bring in two powers of $\ln(Q^2/\Lambda_{QCD}^2)$. Therefore, it (and other graphs not included in Fig. 2.13) is subleading and can be neglected in the LLA.

The contributions of diagrams B and C in Fig. 2.13 to the change in the quark distribution can be calculated directly, similarly to that of diagram A. However, instead of embarking upon another possibly tedious calculation we will derive these contributions using a unitarity argument.

Unitarity argument Let us start with a proton state $|\Psi\rangle$, normalized for simplicity to 1, $\langle\Psi|\Psi\rangle = 1$. Single-gluon corrections of the diagrams in Fig. 2.13 modify the state $|\Psi\rangle$ as follows:

$$|\Psi\rangle \to |\Psi'\rangle = |\Psi\rangle + R|\Psi\rangle + V|\Psi\rangle. \qquad (2.84)$$

Here the new state $|\Psi'\rangle$ consists of a sum of the following terms: (i) the "old" state $|\Psi\rangle$ corresponding to no gluon corrections at all; (ii) the "real" emission shown in Fig. 2.13A,
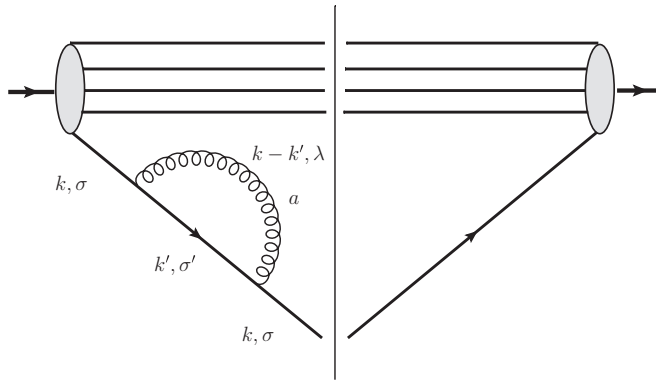
Fig. 2.16. Virtual correction to the quark–quark splitting function.

which turns $|\Psi\rangle$ into $R|\Psi\rangle$ where R denotes the factor relating Ψ_n and Ψ_{n-1} in Eq. (2.74); (iii) the "virtual" emission shown in Figs. 2.13B, C, where the gluon is reabsorbed back into the wave function from which it was emitted, thus leaving the number of partons unchanged and generating a contribution $V|\Psi\rangle$.

Requiring unitarity, i.e., probability conservation $\langle\Psi'|\Psi'\rangle = \langle\Psi|\Psi\rangle = 1$, in Eq. (2.84) leads to

$$R^\dagger R + V + V^* = 0 \qquad (2.85)$$

to order g^2. Therefore, the sum of the contributions of diagrams B and C in Fig. 2.13 is

$$V + V^* = -R^\dagger R. \qquad (2.86)$$

We see that instead of calculating diagrams B and C in Fig. 2.13 we can simply multiply the contribution of diagram A by its conjugate, integrate over the phase space, and sum over the quantum numbers of the produced and measured partons, multiplying the result by -1.

Using the unitarity prescription of Eq. (2.86) along with Eq. (2.77) for the contribution of diagram A, we write the contribution of diagrams B and C from Fig. 2.13 (along with instantaneous terms) as

$$q_{\mathrm{B+C}}^f(x, Q^2) = -\sum_n \int \prod_{i=1}^n \frac{dx_i}{x_i} \frac{d^2k_{i\perp}}{2(2\pi)^3} \frac{1}{x'} \frac{d^2k'_\perp}{2(2\pi)^3} \frac{d(k^+ - k'^+)}{k^+ - k'^+} \frac{d^2k_\perp}{2(2\pi)^3}$$

$$\times 8\pi\alpha_s\, C_F\, \theta(z)\, \theta(1-z) \frac{z(1+z^2)}{k'^2_\perp} \sum_{\sigma=\pm 1} |\Psi_n^f(\{x_i, k_{i\perp}\}; x, k_\perp; \sigma)|^2$$

$$\times (2\pi)^3\, \delta^2\left(\vec{k}_\perp + \sum_{j=1}^n \vec{k}_{j\perp}\right) \delta\left(1 - x - \sum_l^n x_l\right). \qquad (2.87)$$

Equation (2.87) is illustrated in Fig. 2.16. In arriving at Eq. (2.87) we have swapped k and k' as compared with the real emission diagram shown in Fig. 2.14. After emitting a gluon, the

quark now carries momentum k'; the fraction of the light cone momentum of the incoming quark k^+ carried by the quark in the loop is $z = k'^+/k^+$. As above,

$$\int_0^{P^+} \frac{d(k^+ - k'^+)}{k^+ - k'^+} \frac{1}{x'} = \int_0^{k^+} \frac{dk'^+ P^+}{k'^+(k^+ - k'^+)} = \frac{1}{x} \int_0^1 \frac{dz}{z(1-z)}. \tag{2.88}$$

Note that the lower limit of the z-integration in Eq. (2.88) is different from that in Eq. (2.78): this is due to the virtual nature of the diagram in Fig. 2.16. It is also important to remember that now the large transverse momentum is $k'_\perp$, so that $k'^2_\perp \gg k^2_\perp$, which accounts for the factor $k'^2_\perp$ in the denominator in Eq. (2.87).

With the help of Eq. (2.88) and the quark distribution definition (2.65) we can rewrite Eq. (2.87) as

$$q^f_{\mathrm{B+C}}(x, Q^2) = -\frac{\alpha_s C_F}{2\pi} \int^{Q^2} \frac{dk'^2_\perp}{k'^2_\perp} \int_0^1 dz \, \frac{1+z^2}{1-z} q^f(x, k'^2_\perp), \tag{2.89}$$

where, owing to the constraint $k'^2_\perp \gg k^2_\perp$, we may cut off the $k_\perp$-integral in Eq. (2.87) by $k'^2_\perp$ in the UV. The result is that $k'^2_\perp$ is the scale of the quark distribution function on the right-hand side of Eq. (2.89). Note that the $k'_\perp$-integral is a loop integral and is, in general, divergent: it has to be regularized, and so a graph with a counterterm should be added to the diagram in Fig. 2.16. Since Q is the renormalization scale, to leading-logarithmic accuracy we simply cut off the $k'^2_\perp$-integral in Eq. (2.89) by Q^2 in the UV.

Equation (2.89) is the contribution of the virtual diagrams B and C in Fig. 2.13. Just as for the real diagram A, we now imagine that we slowly increase Q^2: the contribution of graphs B and C to the variation in the quark distribution function is

$$Q^2 \frac{\partial q^f_{\mathrm{B+C}}(x, Q^2)}{\partial Q^2} = -\frac{\alpha_s C_F}{2\pi} \int_0^1 dz \, \frac{1+z^2}{1-z} q^f(x, Q^2). \tag{2.90}$$

The total modification of the quark distribution, $\delta q^f(x, Q^2) = \delta q^f_{\mathrm{A}}(x, Q^2) + \delta q^f_{\mathrm{B+C}}(x, Q^2)$, is obtained by summing Eqs. (2.82) and (2.90). This yields

$$Q^2 \frac{\partial q^f(x, Q^2)}{\partial Q^2} = \frac{\alpha_s C_F}{2\pi} \left[\int_x^1 \frac{dz}{z} \frac{1+z^2}{1-z} q^f\left(\frac{x}{z}, Q^2\right) \right.$$
$$\left. - \int_0^1 dz \, \frac{1+z^2}{1-z} q^f(x, Q^2) \right]. \tag{2.91}$$

To write Eq. (2.91) in the standard notation, we define the quark–quark *splitting function* $P_{qq}(z)$ by

$$P_{qq}(z) \equiv C_F \left[\frac{1+z^2}{(1-z)_+} + \frac{3}{2} \delta(1-z) \right] \tag{2.92}$$

with the "plus" notation defined in Sterman (1993),

$$\int\limits_x^1 dz \, \frac{1}{(1-z)_+} \, f(z) = \int\limits_x^1 dz \, \frac{1}{1-z} \, [f(z) - f(1)] + f(1) \ln(1-x), \qquad (2.93)$$

for an arbitrary function $f(z)$ defined for $0 \le x \le 1$. With the help of $P_{qq}(z)$ we rewrite Eq. (2.91) in the more compact form

$$Q^2 \, \frac{\partial q^f(x, Q^2)}{\partial Q^2} = \frac{\alpha_s}{2\pi} \int\limits_x^1 \frac{dz}{z} \, P_{qq}(z) \, q^f\left(\frac{x}{z}, Q^2\right). \qquad (2.94)$$

We have thus obtained a differential equation for the quark distribution function. The initial condition for this equation is usually given by the quark distribution $q^f(x, Q_0^2)$ at some initial virtuality Q_0^2. At low Q_0^2 such an initial condition is likely to be due to some nonperturbative (large-α_s) physics: it cannot be calculated using perturbative techniques and is usually inferred from the data. Given the initial condition $q^f(x, Q_0^2)$, Eq. (2.94) allows one to uniquely construct the quark distribution function at all $Q^2 > Q_0^2$ (with leading-logarithmic accuracy). Therefore Eq. (2.94) *evolves* the quark distribution function in Q^2 from some initial value at Q_0^2 to its value at another scale Q^2: equations like (2.94) are usually referred to as *evolution equations*. The variation of a distribution function with Q^2 is known as the Q^2-*evolution* of the distribution function.

The physical meaning of the splitting function $P_{qq}(z)$ is clear from our derivation of Eq. (2.94): $P_{qq}(z)$ is proportional to the probability of finding one quark in another quark's wave function, with the "measured" quark carrying a fraction z of the original quark's light cone momentum.

Another important question concerns the scale of the coupling constant α_s in Eq. (2.94). Without going into details of the calculation of the running coupling corrections, we simply note that, up to a z-dependent factor, the scale is simply Q^2, so that $\alpha_s = \alpha_s(Q^2)$. Thus the coupling runs with the perturbative (hard) scale of the problem, justifying the use of perturbation theory.

2.4.3 The DGLAP evolution equations

Equation (2.94) is not complete yet: so far we have ignored gluons. Indeed, a quark in the proton's wave function may also result from the splitting of a gluon into a $q\bar{q}$ pair! Thus the gluon distribution $G(x, Q^2)$ also contributes to the modification of the quark distribution. Conversely, the gluon distribution also gets modified owing to the splitting of gluons into gluon pairs, or the emission of gluons from quarks as in Fig. 2.13A.

Including the gluon contribution requires additional calculations, similar to those carried out above. Before outlining these calculations let us first present the result.

We define the *flavor nonsinglet distribution function* by

$$\Delta^{f\bar{f}}(x, Q^2) = q^f(x, Q^2) - q^{\bar{f}}(x, Q^2), \qquad (2.95)$$

where $\bar{f}$ denotes the antiquark of flavor f. Since the splitting of a gluon into $q\bar{q}$ pairs contributes *equally* to the creation of quarks and anti-quarks in the proton's wave function, it should not contribute to the nonsinglet distribution $\Delta^{f\bar{f}}(x, Q^2)$. Hence the evolution of $\Delta^{f\bar{f}}(x, Q^2)$ is driven only by the quark evolution from Eq. (2.94). We thus write

$$Q^2 \frac{\partial \Delta^{f\bar{f}}(x, Q^2)}{\partial Q^2} = \frac{\alpha_s(Q^2)}{2\pi} \int_x^1 \frac{dz}{z} P_{qq}(z) \Delta^{f\bar{f}}\left(\frac{x}{z}, Q^2\right). \tag{2.96}$$

To take the gluon contribution into account we define the *flavor singlet distribution function*

$$\Sigma(x, Q^2) = \sum_f \left[q^f(x, Q^2) + q^{\bar{f}}(x, Q^2) \right]. \tag{2.97}$$

The evolution equations for $\Sigma(x, Q^2)$ and $G(x, Q^2)$ read

$$Q^2 \frac{\partial}{\partial Q^2} \begin{pmatrix} \Sigma(x, Q^2) \\ G(x, Q^2) \end{pmatrix} = \frac{\alpha_s(Q^2)}{2\pi} \int_x^1 \frac{dz}{z} \begin{pmatrix} P_{qq}(z) & P_{qG}(z) \\ P_{Gq}(z) & P_{GG}(z) \end{pmatrix}$$
$$\times \begin{pmatrix} \Sigma(x/z, Q^2) \\ G(x/z, Q^2) \end{pmatrix}. \tag{2.98}$$

Equations (2.96) and (2.98) are known as the Dokshitzer–Gribov–Lipatov–Altarelli–Parisi (DGLAP) evolution equations. The QED version of these equations (involving electrons and photons) in (x, Q^2)-space was originally derived by Gribov and Lipatov (1972), while the QCD version was obtained independently by Altarelli and Parisi (1977) and by Dokshitzer (1977). In the Mellin moment space (to be defined shortly) the QED equations were derived by Christ, Hasslacher, and Mueller (1972) and the QCD equations were derived by Georgi and Politzer (1974) and by Gross and Wilczek (1974).

Equations (2.96) and (2.98) contain the splitting function, $P_{qq}(z)$ from Eq. (2.92), along with three other splitting functions, $P_{qG}(z)$, $P_{Gq}(z)$, and $P_{GG}(z)$. For reference purposes, let us first list all the splitting functions, even though we have already found $P_{qq}(z)$ above. They are

$$P_{qq}(z) = C_F \left[\frac{1 + z^2}{(1 - z)_+} + \frac{3}{2} \delta(1 - z) \right], \tag{2.99a}$$

$$P_{Gq}(z) = C_F \frac{1 + (1 - z)^2}{z}, \tag{2.99b}$$

$$P_{qG}(z) = N_f \left[z^2 + (1 - z)^2 \right], \tag{2.99c}$$

$$P_{GG}(z) = 2N_c \left[\frac{z}{(1 - z)_+} + \frac{1 - z}{z} + z(1 - z) \right] + \frac{11N_c - 2N_f}{6} \delta(1 - z). \tag{2.99d}$$
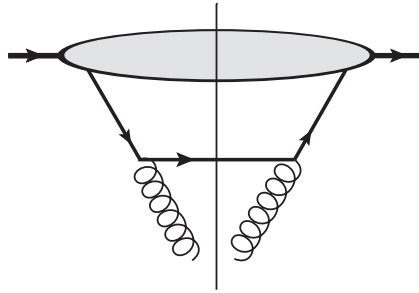
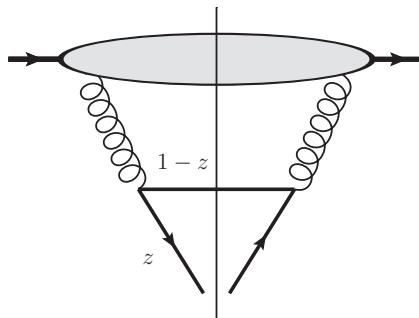Fig. 2.17. The diagram contributing to the splitting function $P_{Gq}(z)$.

Fig. 2.18. The diagram contributing to the splitting function $P_{qG}(z)$.

The "plus" notation is defined above in Eq. (2.93).

The splitting function $P_{Gq}(z)$ is easy to find knowing $P_{qq}(z)$: $P_{Gq}(z)$ represents the probability of finding a gluon in a quark's light cone wave function. Its contribution consists of one diagram, pictured in Fig. 2.17. One can see that the calculation of $P_{Gq}(z)$ would be similar to that of diagram A in Fig. 2.13. The main difference would be in the fact that now it is the gluon that one wants to "measure", and therefore it is the gluon line that carries the longitudinal momentum fraction z of the quark. Since in the calculation of Fig. 2.13A the gluon line carried the momentum fraction $1 - z$, all we have to do to find $P_{Gq}(z)$ is to replace z by $1 - z$ in the contribution of graph A. To single out the contribution of diagram A we need to remove the contributions of the virtual diagrams B and C in Fig. 2.13 from Eq. (2.99a), which is easily accomplished by removing the plus sign in the subscript on the right-hand side and dropping the delta function term, yielding

$$P_{qq}^{real}(z) = C_F \, \frac{1 + z^2}{1 - z}. \tag{2.100}$$

Replacing z by $1 - z$ in $P_{qq}^{real}(z)$ yields $P_{Gq}(z)$, Eq. (2.99b), which is the correct result for the gluon–quark splitting function.

Finding the quark–gluon splitting function $P_{qG}(z)$ is a little more subtle. The only diagram contributing to the splitting function $P_{qG}(z)$ is shown in Fig. 2.18. (One also
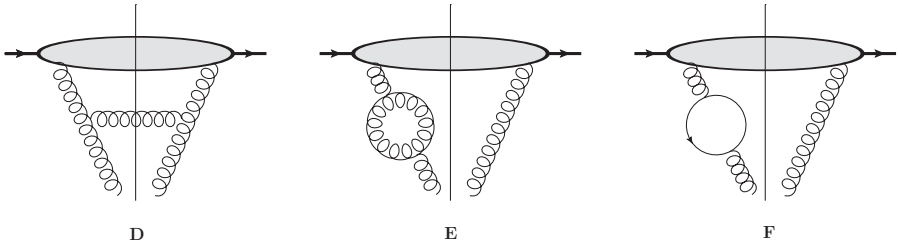
Fig. 2.19. The diagrams contributing to the splitting function $P_{GG}(z)$. The complex conjugates of the last two diagrams (E and F) have to be included in the calculation, along with the instantaneous terms in the quark and gluon propagators in the loops.

has to add in a diagram where we "measure" the antiquark instead of the quark, but the contribution of this diagram is equal to that of the graph in Fig. 2.18.) Comparing this with Fig. 2.14 we see that there are three differences between $P_{qG}(z)$ and the real part of $P_{qq}(z)$: (i) the incoming quark line in Fig. 2.14 becomes an outgoing antiquark line in Fig. 2.18 and the outgoing gluon line in Fig. 2.14 becomes an incoming gluon line in Fig. 2.18; (ii) the color factors are different in the two diagrams; (iii) one has to sum over all quark flavors f and over both quarks and anti-quarks to obtain $P_{qG}(z)$ from Fig. 2.18. Differences (ii) and (iii) are easily addressed. The color factor in Fig. 2.18 is 1/2, which replaces C_F in Eq. (2.99a). The sum over quarks and anti-quarks and over their flavors trivially gives $2N_f$. Hence in the end one has to replace C_F in Eq. (2.99a) by $(1/2) \times 2N_f = N_f$. Difference (i) can be taken into account by applying the crossing symmetry. In the end the prescription is

$$P_{qG}(z) = \frac{N_f}{C_F} z \, P_{qq}^{real} \left(1 - \frac{1}{z} \right), \tag{2.101}$$

which, with the help of $P_{qq}^{real}(z) = C_F(1 + z^2)/(1 - z)$, gives Eq. (2.99c). Indeed, the heuristic derivation of $P_{qG}(z)$ given here needs to be verified by explicit diagrammatic calculations. We leave the explicit calculation of $P_{qG}(z)$ using the diagram in Fig. 2.18 as an exercise for the reader; see Exercise 2.2 at the end of the chapter.

Finding the remaining splitting function $P_{GG}(z)$ requires some explicit diagrammatic calculations as well. We will present them in the next (special-topic) chapter.

2.4.4 Gluon–gluon splitting function*

Our goal here is to derive the gluon–gluon splitting function $P_{GG}(z)$. To calculate $P_{GG}(z)$ one has to sum the graphs shown in Fig. 2.19. There we show only half the diagrams with virtual corrections; the complex conjugates of graphs E and F need to be calculated too. As in the case of the quark–quark splitting function $P_{qq}(z)$, we will calculate only the real emission diagram D in Fig. 2.19 and derive the contributions of the remaining virtual diagrams E and F (and their conjugates) by using unitarity.
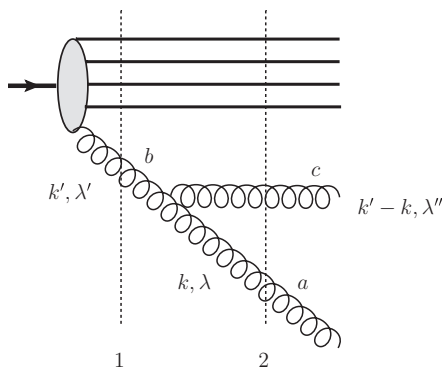
Fig. 2.20. A gluon splitting into two gluons in the proton light cone wave function. As usual, the vertical dotted lines denote intermediate states.

Just as in Sec. 2.4.2, to calculate the graph in Fig. 2.19D for the light cone wave function squared we first need to find the wave function itself. To that end we start with the diagram pictured in Fig. 2.20. Again, the intermediate state 1 is included in the wave function Ψ_{n-1} at the previous step of the evolution. Using the rules of LCPT outlined in Secs. 1.3 and 1.4, we can write the contribution of the graph in Fig. 2.20 as follows:

$$
\Psi_n\left(\{x_i, k_{i\perp}\}; x, k_\perp; \lambda\right) = \frac{i g f^{abc}\theta(k^+)\theta(k'^+ - k^+)}{(k' - k)^- + k^- + \sum_{j=1}^{n-1} k_j^- - P^-} \frac{1}{k'^+}
$$

$$
\times \left[(k' + k) \cdot \epsilon_{\lambda''}^*(k' - k)\, \epsilon_\lambda^*(k) \cdot \epsilon_{\lambda'}(k') + (k - 2k') \cdot \epsilon_\lambda^*(k) \right.
$$

$$
\times \epsilon_{\lambda'}(k') \cdot \epsilon_{\lambda''}^*(k' - k) + (k' - 2k) \cdot \epsilon_{\lambda'}(k')\, \epsilon_{\lambda''}^*(k' - k) \cdot \epsilon_\lambda^*(k) \Big]
$$

$$
\times \Psi_{n-1}\left(\{x_i, k_{i\perp}\}; x', k'_\perp; \lambda'\right), \tag{2.102}
$$

where now $\Psi_n\left(\{x_i, k_{i\perp}\}; x, k_\perp; \lambda\right)$ is the light cone wave function of the proton containing n "spectator" partons and the *gluon* being tagged. As usual $x = k^+/P^+$ and $x' = k'^+/P^+$ are the fractions of the proton's light cone momentum P^+ carried by the gluons.

Using the gluon polarizations in the $A^+ = 0$ light cone gauge,

$$
\epsilon_\mu^\lambda(k) = \left(0, \frac{2\vec{\epsilon}_\perp^\lambda \cdot \vec{k}_\perp}{k^+}, \vec{\epsilon}_\perp^\lambda\right), \tag{2.103a}
$$

$$
\epsilon_\mu^{\lambda'}(k') = \left(0, \frac{2\vec{\epsilon}_\perp^{\lambda'} \cdot \vec{k}'_\perp}{k'^+}, \vec{\epsilon}_\perp^{\lambda'}\right), \tag{2.103b}
$$

$$
\epsilon_\mu^{\lambda''}(k' - k) = \left(0, \frac{2\vec{\epsilon}_\perp^{\lambda''} \cdot (\vec{k}'_\perp - \vec{k}_\perp)}{k'^+ - k^+}, \vec{\epsilon}_\perp^{\lambda''}\right) \tag{2.103c}
$$

with $\vec{\epsilon}_\perp^\lambda = -(1/\sqrt{2})(\lambda, i)$ (and similar expressions involving λ' and λ''), and imposing the transverse momentum ordering $|\vec{k}_\perp| \gg |\vec{k}'_\perp|$ (and, therefore, simply neglecting all terms

containing $\vec{k}'_\perp$), after some straightforward algebra we get

$$(k' + k) \cdot \epsilon^*_{\lambda''}(k' - k) \, \epsilon^*_\lambda(k) \cdot \epsilon_{\lambda'}(k') + (k - 2k') \cdot \epsilon^*_\lambda(k) \, \epsilon_{\lambda'}(k') \cdot \epsilon^*_{\lambda''}(k' - k)$$

$$+ (k' - 2k) \cdot \epsilon_{\lambda'}(k') \, \epsilon^*_{\lambda''}(k' - k) \cdot \epsilon^*_\lambda(k)$$

$$\approx \frac{2}{1 - z} \vec{k}_\perp \cdot \vec{\epsilon}^{\,\lambda''*}_\perp \vec{\epsilon}^{\,\lambda*}_\perp \cdot \vec{\epsilon}^{\,\lambda'}_\perp + \frac{2}{z} \vec{k}_\perp \cdot \vec{\epsilon}^{\,\lambda*}_\perp \vec{\epsilon}^{\,\lambda'}_\perp \cdot \vec{\epsilon}^{\,\lambda''*}_\perp - 2\vec{k}_\perp \cdot \vec{\epsilon}^{\,\lambda'}_\perp \vec{\epsilon}^{\,\lambda*}_\perp \cdot \vec{\epsilon}^{\,\lambda''*}_\perp. \qquad (2.104)$$

Here, as usual, $z = k^+/k'^+$. Using Eqs. (2.104) and (2.73) we can write Eq. (2.102) as

$$\Psi_n \left(\{x_i, k_{i\perp}\}; x, k_\perp; \lambda \right)$$

$$= i g f^{abc} \theta(z) \theta(1 - z) \frac{z(1 - z)}{\vec{k}_\perp^2}$$

$$\times \left(\frac{2}{1 - z} \vec{k}_\perp \cdot \vec{\epsilon}^{\,\lambda''*}_\perp \vec{\epsilon}^{\,\lambda*}_\perp \cdot \vec{\epsilon}^{\,\lambda'}_\perp + \frac{2}{z} \vec{k}_\perp \cdot \vec{\epsilon}^{\,\lambda*}_\perp \vec{\epsilon}^{\,\lambda'}_\perp \cdot \vec{\epsilon}^{\,\lambda''*}_\perp - 2\vec{k}_\perp \cdot \vec{\epsilon}^{\,\lambda'}_\perp \vec{\epsilon}^{\,\lambda*}_\perp \cdot \vec{\epsilon}^{\,\lambda''*}_\perp \right)$$

$$\times \Psi_{n-1} \left(\{x_i, k_{i\perp}\}; x', k'_\perp; \lambda' \right). \qquad (2.105)$$

(We can use Eq. (2.73) since the approximations used in calculating the splitting function $P_{qq}(z)$ are the same as those that we are assuming here for the splitting function $P_{GG}(z)$.)

Multiplying the wave function in Eq. (2.105) by its complex conjugate and summing over polarizations and colors yields

$$\sum_{\lambda, \lambda', \lambda'', a, b, b', c} |\Psi_n \left(\{x_i, k_{i\perp}\}; x, k_\perp; \lambda \right)|^2$$

$$= 16\pi \alpha_s N_c \theta(z) \theta(1 - z) \frac{1}{\vec{k}_\perp^2}$$

$$\times \left[z^2 + (1 - z)^2 + z^2(1 - z)^2 \right] \sum_{\lambda', b} |\Psi_{n-1} \left(\{x_i, k_{i\perp}\}; x', k'_\perp; \lambda' \right)|^2. \qquad (2.106)$$

Note that the definition of the gluon distribution corresponding to Fig. 2.12 implies a summation over the colors of the two gluon lines. The color of the gluon line to the left of the cut is equal to the color of the gluon line to the right of the cut. We have made this color summation explicit in Eq. (2.106) to facilitate the calculation of the color factor: the color of the internal gluon line, which is labeled b in Fig. 2.20, is denoted b' in the complex conjugate wave function. In arriving at Eq. (2.106) we have used $f^{abc} f^{ab'c} = N_c \delta^{bb'}$ and $|\vec{k}_\perp \cdot \vec{\epsilon}^{\,\lambda'}_\perp|^2 = \vec{k}_\perp^2/2$.

Following the steps outlined in Sec. 2.4.2 for the quark distribution function, which led to Eq. (2.80), we infer from Eq. (2.106) that the contribution of diagram D in Fig. 2.19 to

the gluon distribution function is

$$G_{\mathrm{D}}(x, Q^2) = \frac{\alpha_s N_c}{\pi} \frac{1}{x} \int^{Q^2} \frac{dk_\perp^2}{k_\perp^2} \int_x^1 \frac{dz}{z(1-z)} \left[z^2 + (1-z)^2 + z^2(1-z)^2 \right]$$
$$\times x' G(x', k_\perp^2), \tag{2.107}$$

with $z = x/x'$. Again assuming that we are varying Q^2, Eq. (2.107) can be trivially rewritten as

$$Q^2 \frac{\partial G_{\mathrm{D}}(x, Q^2)}{\partial Q^2} = \frac{\alpha_s N_c}{\pi} \int_x^1 \frac{dz}{z} \left[\frac{z}{1-z} + \frac{1-z}{z} + z(1-z) \right] G\left(\frac{x}{z}, Q^2 \right). \tag{2.108}$$

Using the unitarity argument of Sec. 2.4.2 we can calculate the contribution of diagram E in Fig. 2.19 along with its complex conjugate and all the virtual gluon graphs with instantaneous terms (cf. Eq. (2.90)), obtaining

$$Q^2 \frac{\partial G_{\mathrm{E}}(x, Q^2)}{\partial Q^2} = -\frac{\alpha_s N_c}{\pi} \frac{1}{2} \int_0^1 dz \left[\frac{z}{1-z} + \frac{1-z}{z} + z(1-z) \right] G(x, Q^2). \tag{2.109}$$

The factor $1/2$ in Eq. (2.109) is simply a symmetry factor, as the two propagators in the loop of graph E are identical gluons. The z-integration in Eq. (2.109) has two singularities: one at $z = 1$ and the other at $z = 0$. The singularities correspond to either one or the other gluon in the loop of diagram E having a small longitudinal momentum. The two singularities have therefore identical physical origins. We rewrite them as one singularity at $z = 1$:

$$\int_0^1 dz \left[\frac{z}{1-z} + \frac{1-z}{z} + z(1-z) \right] = \int_0^1 dz \left[-1 + \frac{1}{1-z} + \frac{1}{z} - 1 + z(1-z) \right]$$
$$= \int_0^1 dz \left[\frac{2}{1-z} - 2 + z(1-z) \right] = \int_0^1 dz \frac{2}{1-z} - \frac{11}{6}. \tag{2.110}$$

With the help of this rearrangement the sum of diagrams D and E is (cf. Eq. (2.91))

$$Q^2 \frac{\partial G_{\mathrm{D+E}}(x, Q^2)}{\partial Q^2} = \frac{\alpha_s N_c}{\pi} \left\{ \int_x^1 \frac{dz}{z} \left[\frac{z}{1-z} + \frac{1-z}{z} + z(1-z) \right] G\left(\frac{x}{z}, Q^2 \right) \right.$$
$$\left. - \int_0^1 dz \frac{1}{1-z} G(x, Q^2) + \frac{11}{12} G(x, Q^2) \right\}. \tag{2.111}$$

Here we are not going to calculate the contribution of diagram F in Fig. 2.19 explicitly. Instead we will use the splitting function $P_{qG}(z)$ illustrated in Fig. 2.18 and given in

Eq. (2.99c). As one can see from Figs. 2.18 and 2.19, the contribution of graph F in the latter is simply a virtual correction to the diagram in Fig. 2.18. With the help of $P_{qG}(z)$ from Eq. (2.99c) and the unitarity argument of Sec. 2.4.2 we obtain the contribution of diagram F:

$$Q^2 \frac{\partial G_F(x, Q^2)}{\partial Q^2} = -\frac{\alpha_s N_f}{2\pi} \frac{1}{2} \int\limits_0^1 dz \left[z^2 + (1-z)^2 \right] G(x, Q^2). \qquad (2.112)$$

The factor $1/2$ is inserted to remove the double-counting associated with tagging on both the quark and the antiquark in the calculation of $P_{qG}(z)$. Equation (2.112) trivially gives

$$Q^2 \frac{\partial G_F(x, Q^2)}{\partial Q^2} = -\frac{\alpha_s}{2\pi} \frac{N_f}{3} G(x, Q^2). \qquad (2.113)$$

Combining Eqs. (2.111) and (2.113) we arrive at the contribution of all three diagrams in Fig. 2.19:

$$Q^2 \frac{\partial G(x, Q^2)}{\partial Q^2} = \frac{\alpha_s}{2\pi} \left\{ 2N_c \int\limits_x^1 \frac{dz}{z} \left[\frac{z}{1-z} + \frac{1-z}{z} + z(1-z) \right] G\left(\frac{x}{z}, Q^2 \right) \right.$$

$$\left. - 2N_c \int\limits_0^1 dz \frac{1}{1-z} G(x, Q^2) + \frac{11N_c - 2N_f}{6} G(x, Q^2) \right\}. \qquad (2.114)$$

(Even though Eq. (2.114) looks like a closed integro-differential equation, one has to remember that the quark distribution's contribution is not included in its right-hand side and that the full DGLAP evolution for the gluon distribution is given in Eq. (2.98).) Rewriting Eq. (2.114) in the compact form

$$Q^2 \frac{\partial G(x, Q^2)}{\partial Q^2} = \frac{\alpha_s}{2\pi} \int\limits_x^1 \frac{dz}{z} P_{GG}(z) \, G\left(\frac{x}{z}, Q^2 \right), \qquad (2.115)$$

we immediately see that

$$P_{GG}(z) = 2N_c \left[\frac{z}{(1-z)_+} + \frac{1-z}{z} + z(1-z) \right] + \frac{11N_c - 2N_f}{6} \delta(1-z),$$

which is exactly Eq. (2.99d)! We have thus derived the gluon–gluon splitting function.

2.4.5 General solution of the DGLAP equations

To solve the DGLAP equations (2.96) and (2.98), one usually writes them first in *moment space*. The *moment* $f_\omega(Q^2)$ of a distribution function $f(x, Q^2)$ is defined by the Mellin

transform

$$f_\omega(Q^2) \equiv \int\limits_0^1 dx\, x^\omega f(x, Q^2), \tag{2.116}$$

where $f = \Delta^{f\bar{f}}$ or Σ for the nonsinglet or singlet quark distribution functions respectively and $f = G$ for the gluon distribution. Inverting Eq. (2.116), we write the distribution function as

$$f(x, Q^2) = \int\limits_{a-i\infty}^{a+i\infty} \frac{d\omega}{2\pi i} x^{-\omega-1} f_\omega(Q^2), \tag{2.117}$$

where the integral in ω-space runs along a contour parallel to the imaginary axis and to the right of all the singularities of the moment $f_\omega(Q^2)$ (which can be chosen by adjusting the arbitrary real number a).

As one can show (see Exercise 2.5), in the moment space the DGLAP equations (2.96) and (2.98) become

$$Q^2 \frac{\partial \Delta_\omega^{f\bar{f}}(Q^2)}{\partial Q^2} = \frac{\alpha_s(Q^2)}{2\pi} \gamma_{qq}(\omega) \Delta_\omega^{f\bar{f}}(Q^2) \tag{2.118}$$

and

$$Q^2 \frac{\partial}{\partial Q^2} \begin{pmatrix} \Sigma_\omega(Q^2) \\ G_\omega(Q^2) \end{pmatrix} = \frac{\alpha_s(Q^2)}{2\pi} \begin{pmatrix} \gamma_{qq}(\omega) & \gamma_{qG}(\omega) \\ \gamma_{Gq}(\omega) & \gamma_{GG}(\omega) \end{pmatrix} \begin{pmatrix} \Sigma_\omega(Q^2) \\ G_\omega(Q^2) \end{pmatrix}. \tag{2.119}$$

In arriving at Eqs. (2.118) and (2.119) we have defined *anomalous dimensions* $\gamma_{ij}(\omega)$ by

$$\gamma_{ij}(\omega) = \int\limits_0^1 dz\, z^\omega P_{ij}(z), \tag{2.120}$$

where i, j can each be equal to either q or G. With the help of Eqs. (2.99) and (2.120) one can show that the DGLAP anomalous dimensions are (Georgi and Politzer 1974, Gross and Wilczek 1974)

$$\gamma_{qq}(\omega) = C_F \left[\frac{3}{2} + \frac{1}{(1+\omega)(2+\omega)} - 2\psi(\omega+2) + 2\psi(1) \right], \tag{2.121a}$$

$$\gamma_{Gq}(\omega) = C_F \left[\frac{1}{2+\omega} + \frac{2}{\omega(1+\omega)} \right], \tag{2.121b}$$

$$\gamma_{qG}(\omega) = N_f \left[\frac{1}{1+\omega} - \frac{2}{(2+\omega)(3+\omega)} \right], \tag{2.121c}$$

$$\gamma_{GG}(\omega) = \frac{11N_c - 2N_f}{6}$$
$$+ 2N_c \left[\frac{1}{\omega(1+\omega)} + \frac{1}{(2+\omega)(3+\omega)} - \psi(\omega+2) + \psi(1) \right], \tag{2.121d}$$
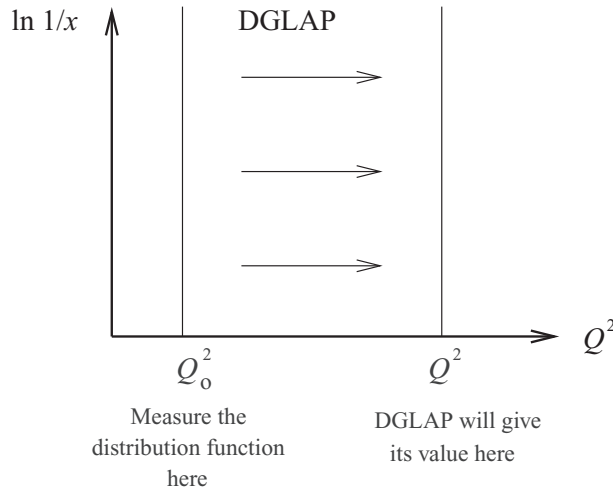
Fig. 2.21. The DGLAP equations in the ($\ln 1/x$, Q^2)-plane.

where $\psi(w) = \Gamma'(w)/\Gamma(w)$ is the digamma function. Note that $\psi(1) = -\gamma_E$, with γ_E Euler's constant. We leave the derivation of the anomalous dimensions (2.121) as an exercise; see Exercise 2.5.

Equations (2.118) and (2.119) are easy to solve. Suppose that the (usually nonperturbative) initial conditions for the equations are given at some initial scale Q_0^2. That is, we know $\Delta^{f\bar{f}}(x, Q_0^2)$, $\Sigma(x, Q_0^2)$, and $G(x, Q_0^2)$. Using Eq. (2.116) we can find the initial conditions for the moments, obtaining $\Delta_\omega^{f\bar{f}}(Q_0^2)$, $\Sigma_\omega(Q_0^2)$, and $G_\omega(Q_0^2)$. Solving Eqs. (2.118) and (2.119) we can now find the moments of the distribution functions at all Q^2:

$$\Delta_\omega^{f\bar{f}}(Q^2) = \exp\left\{\int_{Q_0^2}^{Q^2} \frac{dQ'^2}{Q'^2} \frac{\alpha_s(Q'^2)}{2\pi} \gamma_{qq}(\omega)\right\} \Delta_\omega^{f\bar{f}}(Q_0^2), \tag{2.122}$$

$$\begin{pmatrix} \Sigma_\omega(Q^2) \\ G_\omega(Q^2) \end{pmatrix} = \exp\left\{\int_{Q_0^2}^{Q^2} \frac{dQ'^2}{Q'^2} \frac{\alpha_s(Q'^2)}{2\pi} \begin{pmatrix} \gamma_{qq}(\omega) & \gamma_{qG}(\omega) \\ \gamma_{Gq}(\omega) & \gamma_{GG}(\omega) \end{pmatrix}\right\} \begin{pmatrix} \Sigma_\omega(Q_0^2) \\ G_\omega(Q_0^2) \end{pmatrix}. \tag{2.123}$$

Equations (2.122) and (2.123) allow one to find the distribution functions in moment space. With the help of Eq. (2.117) one then can transform the moments of the distribution functions back into x-space, thus obtaining the distribution functions solving the DGLAP equations at all Q^2.

The way in which the DGLAP equations work is depicted in Fig. 2.21 in the ($\ln 1/x$, Q^2)-plane, which we will often use to demonstrate our results. The initial values of the distribution functions for DGLAP evolution are set at some initial scale Q_0^2 for all the relevant values of x: thus the initial conditions are given along the vertical line on the left in Fig. 2.21. Given the initial conditions, the DGLAP equations then give the distribution functions at other values of Q^2. For instance, using the DGLAP equations one may obtain

distribution functions along the vertical line on the right in Fig. 2.21. Thus the DGLAP equations *evolve* the distribution functions in Q^2 from some initial conditions at Q_0^2 to their values at some other Q^2, as indicated by the arrows in Fig. 2.21. Note that the curves shown in Fig. 2.7 resulted from using the DGLAP equations, having adjusted the initial conditions to fit the DIS data.

Indeed the DGLAP equations (2.98) and (2.96) presented above are valid only at the leading-logarithmic level. They are often referred to as the leading-order (LO) DGLAP equations, since the integral kernel on the right-hand side is given at the lowest order in α_s (i.e., at order α_s). Higher-order corrections to the splitting functions would generate terms with higher powers of α_s on the right-hand sides of Eqs. (2.98) and (2.96). For instance Eqs. (2.98) and (2.96), with right-hand sides calculated up to $O(\alpha_s^2)$, are referred to as next-to-leading-order DGLAP or simply NLO DGLAP. The next order after that is called next-to-next-to-leading-order DGLAP (NNLO DGLAP), etc. Note that at such higher orders the naive factorization relations (2.45) and (2.46) (see also Eq. (2.48)) between the structure functions and the quark distribution function would be modified. Even the LO DGLAP evolution of Eqs. (2.98) and (2.96) obviously violates Bjorken scaling. It also generates corrections to the Callan–Gross relation (2.44).

2.4.6 Double logarithmic approximation

Let us now study structure functions and parton distributions at small Bjorken x using the DGLAP equations. This limit is interesting and important for our discussion, since small x corresponds to high energy $\hat{s}$ of virtual photon–proton scattering, as one can see from Eqs. (2.6). A brief inspection of Fig. 2.7 shows that the structure function F_2 clearly rises at small x. The question that we would like to address is whether DGLAP evolution can provide a theoretical explanation for such a rise.

To answer this question we need to analyze Eqs. (2.96) and (2.98) at small x. At small x the z-integral in Eqs. (2.96) and (2.98) may get extra enhancement from the small-z region. To see this let us study the small-z asymptotics of the splitting functions. Using Eqs. (2.99) one can show that only two of the splitting functions are singular at small z:

$$P_{Gq}(z)\bigg|_{z\ll 1} \approx \frac{2C_F}{z}, \quad P_{GG}(z)\bigg|_{z\ll 1} \approx \frac{2N_c}{z}. \tag{2.124}$$

Thus, in Eqs. (2.96) and (2.98) only the second line of Eq. (2.98) is enhanced at small x. We conclude that the evolution of the gluon distribution $G(x, Q^2)$ runs much faster than that of the quark distributions (both singlet and nonsinglet), at small x. Therefore we can neglect the evolution of the quark distribution functions compared with that of the gluon. Also, the quark contribution to the gluon evolution, which enters via $P_{Gq}(z)$ into Eq. (2.98), is negligible as well: as $\Sigma(x, Q^2)$ is small owing to the lack of small-x enhancement to its own evolution, it would not contribute much to the gluon evolution.

Neglecting the quark distribution in the DGLAP equation (2.98) and using the approximation for the gluon–gluon splitting function from Eq. (2.124), we can write down an

evolution equation for the gluon distribution only,

$$Q^2 \frac{\partial G(x, Q^2)}{\partial Q^2} = \frac{\alpha_s(Q^2)}{2\pi} \int\limits_x^1 \frac{dz}{z} \frac{2N_c}{z} G\left(\frac{x}{z}, Q^2\right), \tag{2.125}$$

which of course is valid only at small x.

Before we solve Eq. (2.125), let us clarify the approximation that we have made in arriving at this equation. To see this more clearly, let us redefine z as x/x' and write Eq. (2.125) as

$$Q^2 \frac{\partial x G(x, Q^2)}{\partial Q^2} = \frac{\alpha_s(Q^2) N_c}{\pi} \int\limits_x^1 \frac{dx'}{x'} x' G(x', Q^2). \tag{2.126}$$

Differentiating Eq. (2.126) with respect to $\ln(1/x)$, we can write it as

$$\frac{\partial^2 x G(x, Q^2)}{\partial \ln(1/x) \partial \ln(Q^2/Q_0^2)} = \frac{\alpha_s(Q^2) N_c}{\pi} x G(x, Q^2) \tag{2.127}$$

with Q_0 a constant initial-virtuality scale.

For simplicity let us imagine that the coupling constant is fixed, $\alpha_s(Q^2) = \alpha_s$. We can then see clearly from Eq. (2.127) that its solution iterates powers of α_s multiplied not just by one logarithm, $\ln(Q^2/Q_0^2)$, as in the DGLAP equations, but by two logarithms, $\ln(1/x) \ln(Q^2/Q_0^2)$. Thus the resummation parameter of Eq. (2.127) is

$$\alpha_s \ln \frac{1}{x} \ln \frac{Q^2}{Q_0^2}. \tag{2.128}$$

Thus at small coupling $\alpha_s \ll 1$, large $Q^2 \gg Q_0^2$, and small x such that $\ln(1/x) \gg 1$, we see that the small coupling α_s is multiplied by two large logarithms, which makes the resummation parameter (2.128) large and important to resum. Resummation of a series in powers of the parameter (2.128) is called the double logarithmic approximation (DLA).

With the DLA parameter (2.128) the approximations we made in obtaining Eq. (2.125) become clear. The absence of $1/z$ singularities in $P_{qq}(z)$ and $P_{qG}(z)$ insures that no $\ln(1/x)$ factor is generated in each step of the DGLAP evolution for the singlet and nonsinglet quark structure functions. Hence the evolution of $\Sigma(x, Q_0^2)$ and of $\Delta^{f\bar{f}}(x, Q_0^2)$ is subleading in the DLA parameter (2.128) and can be neglected in the approximation that resums only powers of the logarithms of both Q^2 and $1/x$ in Eq. (2.128).

Now let us solve Eq. (2.125). Substituting the approximate gluon–gluon splitting function from Eq. (2.124) into Eq. (2.120) we obtain

$$\gamma_{GG}(\omega) \approx \frac{2N_c}{\omega}. \tag{2.129}$$

One can see that the small-z singularity in $P_{GG}(z)$ translates into a singularity at $\omega = 0$ in $\gamma_{GG}(\omega)$. This is an important result, which we will use below.

With the help of Eq. (2.129) we can write Eq. (2.125) in moment space:

$$Q^2 \frac{\partial G_\omega(Q^2)}{\partial Q^2} = \frac{\alpha_s(Q^2) N_c}{\pi} \frac{1}{\omega} G_\omega(Q^2). \tag{2.130}$$

From Eqs. (2.121) one can see that only $\gamma_{GG}(\omega)$ and $\gamma_{Gq}(\omega)$ have singularities at $\omega = 0$: using this observation we could have derived the DLA DGLAP evolution equation in moment space (2.130) directly from Eq. (2.119).

The solution of Eq. (2.130) is easily found and reads

$$G_\omega(Q^2) = \exp\left\{ \int_{Q_0^2}^{Q^2} \frac{dQ'^2}{Q'^2} \frac{\alpha_s(Q'^2)N_c}{\pi\omega} \right\} G_\omega(Q_0^2). \tag{2.131}$$

Inverting the Mellin transform (2.116) with the help of Eq. (2.117), we obtain the gluon distribution function in the DLA:

$$xG(x, Q^2) = \int_{a-i\infty}^{a+i\infty} \frac{d\omega}{2\pi i} \exp\left\{ \omega \ln\frac{1}{x} + \int_{Q_0^2}^{Q^2} \frac{dQ'^2}{Q'^2} \frac{\alpha_s(Q'^2)N_c}{\pi\omega} \right\} G_\omega(Q_0^2). \tag{2.132}$$

The Q'^2-integral is easy to carry out. Taking the one-loop running coupling constant

$$\alpha_s(Q^2) = \frac{1}{\beta_2 \ln(Q^2/\Lambda_{QCD}^2)}$$

and assuming that $Q_0^2 > \Lambda_{QCD}^2$, we can write Eq. (2.132) as

$$xG(x, Q^2) = \int_{a-i\infty}^{a+i\infty} \frac{d\omega}{2\pi i} \exp\left\{ \omega \ln\frac{1}{x} + \frac{N_c}{\pi\beta_2\omega} \ln\frac{\ln(Q^2/\Lambda_{QCD}^2)}{\ln(Q_0^2/\Lambda_{QCD}^2)} \right\} G_\omega(Q_0^2). \tag{2.133}$$

Note that, with the inclusion of the running coupling corrections, the transverse logarithm $\ln(Q^2/Q_0^2)$ in Eq. (2.128) turns into the logarithm of the ratio of logarithms seen in the exponent of Eq. (2.133).

The integral in Eq. (2.133) cannot be calculated exactly without explicit knowledge of the initial conditions, which give $G_\omega(Q_0^2)$. However, it can be evaluated approximately for very small x and very large Q^2 using the saddle point (steepest descent) approximation. To do so we rewrite Eq. (2.133) as

$$xG(x, Q^2) = \int_{a-i\infty}^{a+i\infty} \frac{d\omega}{2\pi i} e^{P(\omega)} G_\omega(Q_0^2) \tag{2.134}$$

with all the x- and Q^2-dependent terms assembled in the exponent:

$$P(\omega) = \omega \ln\frac{1}{x} + \frac{N_c}{\pi\beta_2\omega} \rho(Q^2), \tag{2.135}$$

where we have defined an abbreviated notation

$$\rho(Q^2) \equiv \ln\frac{\ln(Q^2/\Lambda_{QCD}^2)}{\ln(Q_0^2/\Lambda_{QCD}^2)} = \ln\frac{\alpha_s(Q_0^2)}{\alpha_s(Q^2)}. \tag{2.136}$$

Indeed, $P(\omega)$ is also a function of x and Q^2: we have suppressed these arguments for brevity.

First we need to find the saddle points of the exponent $P(\omega)$, which are defined by the condition

$$P'(\omega = \omega_{sp}) = 0, \tag{2.137}$$

where the prime denotes a (partial) derivative with respect to ω. For $P(\omega)$ from Eq. (2.135) we get the saddle points

$$\omega_{sp} = \pm \sqrt{\frac{N_c}{\pi \beta_2} \frac{\rho(Q^2)}{\ln(1/x)}}. \tag{2.138}$$

One can easily argue that at small x the saddle point with the plus sign in Eq. (2.138) dominates. From here on we will label by ω_{sp} the expression in Eq. (2.138) with the plus sign.

Our next step is to approximate the exponent $P(\omega)$ by its Taylor expansion around the saddle point up to the quadratic term:

$$P(\omega) \approx P(\omega_{sp}) + \tfrac{1}{2} P''(\omega_{sp})(\omega - \omega_{sp})^2, \tag{2.139}$$

where the term linear in $\omega - \omega_{sp}$ is zero owing to the condition (2.137). Since $P''(\omega_{sp})$ is real and positive, distorting the integration contour in Eq. (2.134) so that it goes through ω_{sp} when crossing the real axis in the complex ω-plane (i.e., setting $a = \omega_{sp}$), we can define a new integration variable w by

$$\omega - \omega_{sp} \equiv i w. \tag{2.140}$$

Note that w is real along the new integration contour.

With this contour distortion and variable redefinition, Eq. (2.134) becomes

$$x G(x, Q^2) \approx e^{P(\omega_{sp})} G_{\omega_{sp}}(Q_0^2) \int\limits_{-\infty}^{\infty} \frac{dw}{2\pi} e^{-P''(\omega_{sp})w^2/2}, \tag{2.141}$$

where we also assume that G_ω is a slowly varying function of ω such that, owing to saddle point dominance, $G_\omega(Q_0^2) \approx G_{\omega_{sp}}(Q_0^2)$. Performing w-integration yields

$$x G(x, Q^2) \approx \frac{G_{\omega_{sp}}(Q_0^2)}{\sqrt{2\pi P''(\omega_{sp})}} e^{P(\omega_{sp})}. \tag{2.142}$$

With the help of Eqs. (2.138) (with the plus sign), (2.135), and (4.176) we obtain the DLA gluon distribution function in the saddle point approximation,

$$x G(x, Q^2) \approx \frac{G_{\omega_{sp}}(Q_0^2)}{\sqrt{4\pi}} \left\{ \frac{N_c}{\pi \beta_2} \ln \frac{\ln(Q^2/\Lambda_{QCD}^2)}{\ln(Q_0^2/\Lambda_{QCD}^2)} \right\}^{1/4} \left(\ln \frac{1}{x} \right)^{-3/4}$$

$$\times \exp \left\{ 2 \sqrt{\frac{N_c}{\pi \beta_2} \ln \frac{\ln(Q^2/\Lambda_{QCD}^2)}{\ln(Q_0^2/\Lambda_{QCD}^2)} \ln \frac{1}{x}} \right\}. \tag{2.143}$$

To justify the expansion (2.139) that led ultimately to Eq. (2.143) we need to estimate the next (cubic) term in the expansion, which previously we neglected:

$$P'''(\omega_{sp})(\omega - \omega_{sp})^3. \tag{2.144}$$

Since in the integral in Eq. (2.141) the typical width is

$$\omega - \omega_{sp} \sim \frac{1}{\sqrt{P''(\omega_{sp})}}, \tag{2.145}$$

we see that

$$P'''(\omega_{sp})(\omega - \omega_{sp})^3 \sim P'''(\omega_{sp})[P''(\omega_{sp})]^{-3/2}. \tag{2.146}$$

Using Eqs. (2.138) and (2.135) one can readily show that

$$P'''(\omega_{sp})(\omega - \omega_{sp})^3 \sim \left[\rho(Q^2)\right]^{-1/4} \left(\ln \frac{1}{x}\right)^{-1/4}, \tag{2.147}$$

which is negligibly small at small x and large Q^2, justifying our approximation.

Our main result from Eq. (2.143) is that

$$xG(x, Q^2) \sim \exp \left\{ 2 \sqrt{\frac{N_c}{\pi \beta_2} \ln \frac{\ln(Q^2/\Lambda_{QCD}^2)}{\ln(Q_0^2/\Lambda_{QCD}^2)} \ln \frac{1}{x}} \right\}. \tag{2.148}$$

That is, $xG(x, Q^2)$ increases as x decreases and/or Q^2 increases. The rise in $xG(x, Q^2)$ with decreasing x is therefore a prediction of the DGLAP evolution. As we can see from Eq. (2.148), the DGLAP equation predicts a rise in $xG(x, Q^2)$ with decreasing x that is faster than any power of $\ln(1/x)$ but is slower than a power of $1/x$. A rising gluon distribution would translate into a rising (but smaller) quark distribution; both would lead to an increase in the structure function $F_2(x, Q^2)$ at small x, which is in (at least) qualitative agreement with the data in Fig. 2.7. A detailed analysis of the DIS data shows that DGLAP-based fits are able to describe most data (after a suitable choice of initial conditions is made), as demonstrated by the curves in Fig. 2.7.

A physical picture of DGLAP evolution is shown in Fig. 2.22 using the transverse plane representation of the proton from Fig. 2.8. On the left of Fig. 2.22 we show a proton with partons in it, as seen by a virtual photon with virtuality Q_0 corresponding to the resolution scale $1/Q_0$ in the transverse plane. On the right we show what happens when the same proton is probed by a virtual photon with higher virtuality, $Q > Q_0$, which is able to resolve shorter transverse distances $1/Q$. When probing the partons (quarks) at shorter distances the photon is able to distinguish that each quark may fluctuate into itself along with, say, several gluons and/or quark–antiquark pairs, as we see from the DGLAP splitting functions. The net number of partons at the higher scale Q is thus larger than at the scale Q_0, in agreement with the prediction from Eq. (2.148). To illustrate how the DGLAP equation works in practice, we will present some distribution functions extracted from DIS experiments on protons. One usually distinguishes contributions to the quark distribution function coming from the valence quarks (the two u quarks and the d quark in the proton) and from the sea quarks (all the other quarks in the proton).
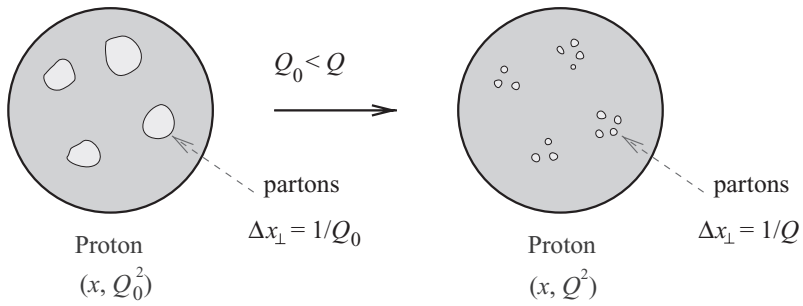
Fig. 2.22. A graphical illustration of the DGLAP evolution equations. The blobs indicate partons (quarks and gluons). A color version of this figure is available online at www.cambridge.org/9780521112574.
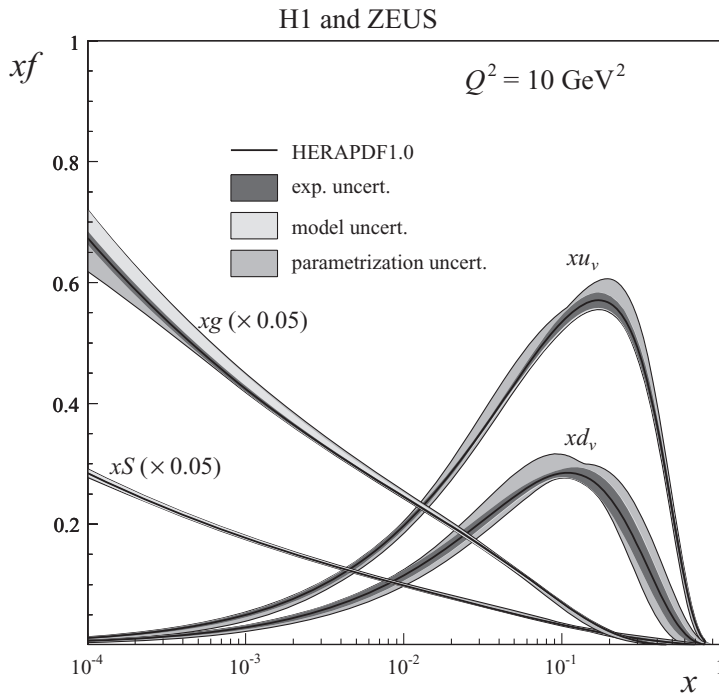

Fig. 2.23. Valence and sea quark distributions in the proton, plotted along with the gluon distribution, as functions of Bjorken x for fixed $Q^2 = 10$ GeV^2. (Reprinted with kind permission from Springer Science +Business Media: H1 and ZEUS collaboration (2010).) A color version of this figure is available online at www.cambridge.org/9780521112574.

Figure 2.23 shows the valence quark distributions $xu_v(x, Q^2)$ and $xd_v(x, Q^2)$, along with the sea quark distribution xS and the gluon distribution xg. All distributions are plotted as functions of x for fixed $Q^2 = 10$ GeV^2. The curves in Fig. 2.23 are the result of a combined NLO DGLAP-based fit of the data from the H1 and ZEUS collaborations at DESY (H1
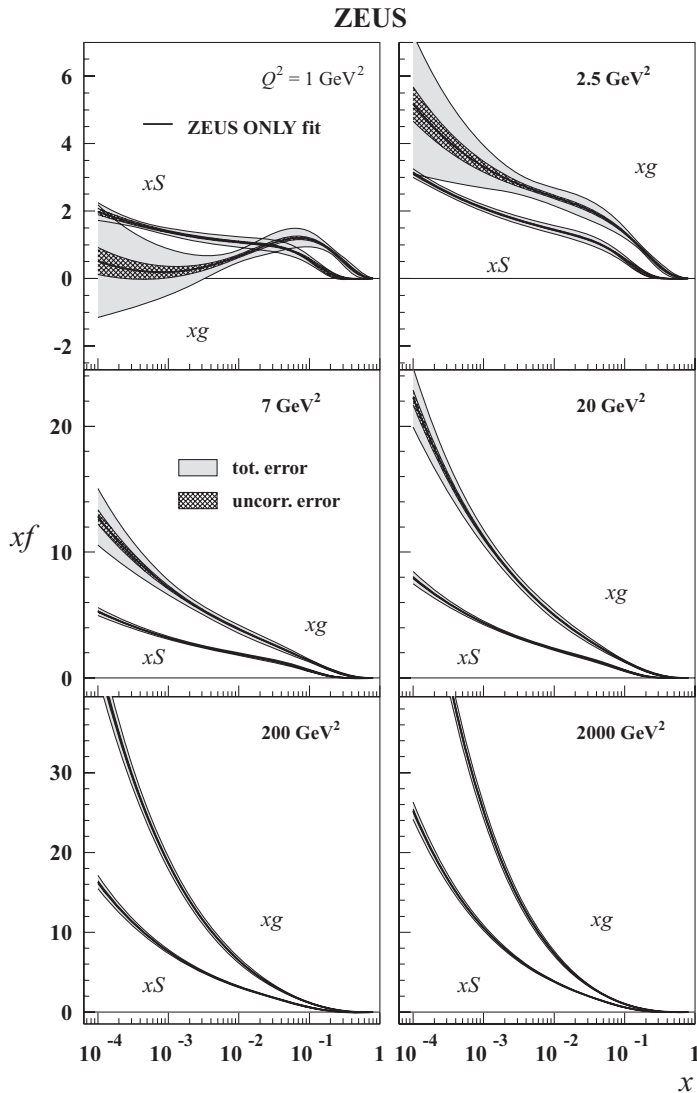
ZEUS

Fig. 2.24. Gluon and sea quark distributions in the proton plotted as functions of Bjorken x for six different values of Q^2. (Reprinted with permission from ZEUS collaboration (2003). Copyright 2003 by the American Physical Society.) A color version of this figure is available online at www.cambridge.org/9780521112574.

and ZEUS collaboration 2010). Note that the sea quark and gluon distributions were scaled down by a factor 0.05 to fit into the same plot as the valence quark distributions. One can see clearly that the gluon and sea quark distributions dominate at small x, in qualitative agreement with the DLA DGLAP predictions.

In Fig. 2.24 we give the sea quark and gluon distributions as functions of x for six different values of Q^2. The curves in Fig. 2.24 are the results of an NLO DGLAP-based
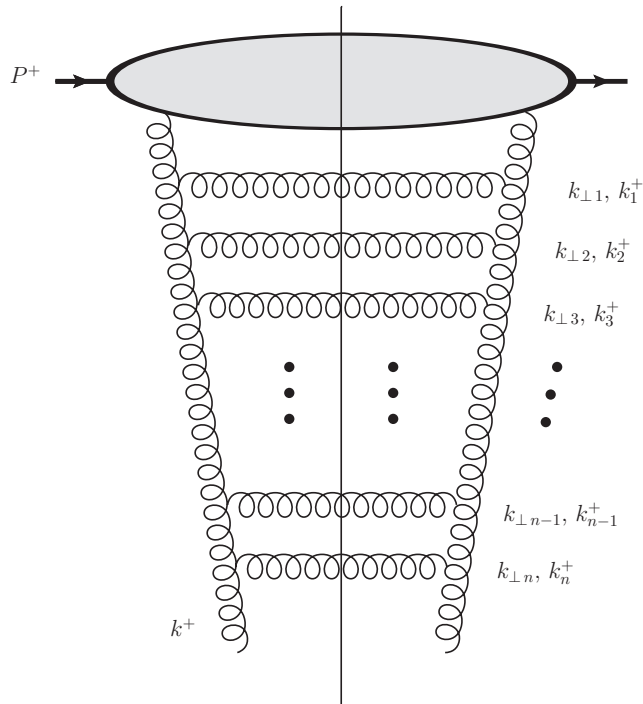
Fig. 2.25. An example of a ladder diagram contributing to DLA DGLAP evolution for the gluon distribution function. The momenta of the gluons in the rungs of the ladder are labeled on the right. The incoming proton has light cone momentum P^+, and the last t-channel gluon in the ladder has light cone momentum k^+.

fit to the DIS data performed by the ZEUS collaboration at HERA (ZEUS collaboration 2003). The initial condition for DGLAP evolution was set at $Q_0^2 = 1 \text{ GeV}^2$. Again one can see that at small x the gluon distribution dominates the quark distributions. In agreement with the DGLAP-based prediction, we see that the gluons play the most important role at small x.

In closing the chapter we will rederive Eq. (2.148) using a more diagram-based approach. Let us construct the solution for the DLA DGLAP evolution equation for the gluon distribution (2.125) by summing diagrams that iterate the kernel of the evolution equation given by the real part of the gluon–gluon splitting function in Fig. 2.19D. (Note that the parts of the splitting functions that are singular at small z, given by Eq. (2.124), are entirely due to the real emission diagrams). Diagrams iterating the gluon emission kernel have a "ladder" structure, as shown in Fig. 2.25. There the transverse momenta of the gluons in the rungs of the ladder, when ordered as

$$k_{\perp n}^2 \gg k_{\perp n-1}^2 \gg \cdots \gg k_{\perp 2}^2 \gg k_{\perp 1}^2 \qquad (2.149)$$

give the transverse logarithms of DGLAP evolution. As we are interested in the DLA limit, the longitudinal momenta of the gluons in Fig. 2.25 can be ordered too, as

$$k_1^+ \gg k_2^+ \gg \cdots \gg k_{n-1}^+ \gg k_n^+ \gg k^+, \tag{2.150}$$

to generate the logarithms of x. Each rung of the ladder generates a logarithmic integral over longitudinal momenta dk^+/k^+, a logarithmic integral over transverse momenta $dk_\perp^2/k_\perp^2$, and a power of the coupling constant $\alpha_s(k_\perp^2)$. Each rung also brings in a color factor N_c and a factor $1/\pi$ coming from more careful diagram evaluation, which we will not perform here. Ordering all the integrations, we get

$$xG(x, Q^2) \sim \sum_{n=0}^{\infty} \int_{Q_0^2}^{Q^2} \frac{dk_{\perp n}^2}{k_{\perp n}^2} \, \bar{\alpha}_s(k_{\perp n}^2) \int_{Q_0^2}^{k_{\perp n}^2} \frac{dk_{\perp n-1}^2}{k_{\perp n-1}^2} \bar{\alpha}_s(k_{\perp n-1}^2) \cdots$$

$$\times \int_{Q_0^2}^{k_{\perp 2}^2} \frac{dk_{\perp 1}^2}{k_{\perp 1}^2} \, \bar{\alpha}_s(k_{\perp 1}^2) \int_{k^+}^{P^+} \frac{dk_1^+}{k_1^+} \int_{k^+}^{k_1^+} \frac{dk_2^+}{k_2^+} \cdots \int_{k^+}^{k_{n-1}^+} \frac{dk_n^+}{k_n^+}, \tag{2.151}$$

where

$$\bar{\alpha}_s(Q^2) \equiv \frac{\alpha_s(Q^2) N_c}{\pi}. \tag{2.152}$$

Performing the integrals yields (as $x = k^+/P^+$)

$$xG(x, Q^2) \sim \sum_{n=0}^{\infty} \frac{1}{(n!)^2} \left[\int_{Q_0^2}^{Q^2} \frac{dk_\perp^2}{k_\perp^2} \, \bar{\alpha}_s(k_\perp^2) \ln \frac{1}{x} \right]^n \tag{2.153}$$

or, equivalently,

$$xG(x, Q^2) \sim \sum_{n=0}^{\infty} \frac{1}{(n!)^2} \left[\frac{N_c}{\pi \beta_2} \rho(Q^2) \ln \frac{1}{x} \right]^n, \tag{2.154}$$

which after summation gives a modified Bessel function:

$$xG(x, Q^2) \sim I_0 \left(2 \sqrt{\frac{N_c}{\pi \beta_2} \rho(Q^2) \ln \frac{1}{x}} \right). \tag{2.155}$$

The exact index of the modified Bessel function depends on the initial conditions for the evolution and is not always 0 (Gorshkov *et al.* 1968). Using the large-argument asymptotics of the modified Bessel function, $I_\nu(z) \sim e^z$, we obtain Eq. (2.148). The prefactor in front of the exponent, shown in Eq. (2.143), can be obtained similarly, by keeping the prefactor in the asymptotics of the modified Bessel function and matching the initial conditions to those used in obtaining Eq. (2.143).

The derivation we have presented shows the diagrammatic origin of the result (2.148). Diagrams also allow one to understand the space–time structure of the parton emissions.

Consider the proton in Fig. 2.25, which, as throughout this chapter, is moving in the light cone plus direction. The light cone times of gluon emissions, which we label x_i^+ for the ith gluon shown in the ladder in Fig. 2.25, owing to the uncertainty principle are given by $x_i^+ \approx 1/k_i^-$. As the gluons in the rungs of the ladder are on mass shell, $k_i^- = k_{\perp i}^2/k_i^+$ and $x_i^+ \approx k_i^+/k_{\perp i}^2$. The DGLAP ordering of transverse momenta (2.149) of itself insures that

$$x_1^+ \gg x_2^+ \gg \cdots \gg x_n^+. \tag{2.156}$$

The ordering of longitudinal momenta (2.150) merely reinforces the ordering of gluon lifetimes (2.156). We see that the gluons with the lowest transverse momentum and/or largest longitudinal momentum are emitted earliest and have the longest lifetimes. Conversely the gluons with the largest transverse momenta and/or smallest longitudinal momenta are emitted last and exist over the shortest lifetimes. This time-ordering of gluon emissions is not only important for our understanding of DGLAP evolution, but will be useful when we start talking about the small-x evolution equations, as it applies there too.

Further reading

A detailed pedagogical discussion of DIS and the DGLAP evolution equations covering topics omitted in this chapter can be found in Halzen and Martin (1984), Sterman (1993), Peskin and Schroeder (1995), Ellis, Stirling, and Webber (1996), and Weinberg (1996).

The reader can find NLO splitting functions for DGLAP evolution in Ellis, Stirling, and Webber (1996). For further discussion of the running coupling scale in DGLAP evolution we refer the reader to Dokshitzer and Shirkov (1995).

Exercises

2.1 Show that, in general, the hadronic tensor $W^{\mu\nu}(p, q)$ can be written in the form (2.16). Do this by observing that it is a function of two four-vectors p^μ and q^μ only, demanding that $W^{\mu\nu}$ is symmetric ($W^{\mu\nu} = W^{\nu\mu}$), and imposing the conditions (2.15).

2.2[*] Calculate the splitting function $P_{qG}(z)$ in light cone perturbation theory using the diagram in Fig. 2.18. You should get Eq. (2.99c).

2.3 Show that the DGLAP equations conserve the longitudinal momentum of the partons. Starting from Eq. (2.98), and using Eqs. (2.99), show that

$$\int\limits_0^1 dx \, x \left[\Sigma(x, Q^2) + G(x, Q^2) \right] \tag{2.157}$$

is independent of Q^2. With the help of Eq. (2.119) argue that this momentum conservation requires that all the anomalous dimensions are zero at $\omega = 1$, i.e., $\gamma_{ij}(\omega = 1) = 0$.

2.4 Show that the DGLAP equations conserve baryon number. Starting from Eq. (2.96), and using Eq. (2.99a), show that

$$\int_0^1 dx \, \Delta^{f\bar{f}}(x, Q^2) \tag{2.158}$$

is independent of Q^2.

2.5 (a) Starting from Eqs. (2.96) and (2.98), and with the help of Eq. (2.116), derive the DGLAP equations in moment space, obtaining Eqs. (2.118) and (2.119) with the anomalous dimensions defined in Eq. (2.120).

    (b) Explicitly derive the DGLAP anomalous dimensions shown above in Eqs. (2.121): that is, use Eq. (2.120) to integrate the splitting functions given by Eqs. (2.99).

2.6 Using the methods in Sec. 2.4.6, solve the DGLAP equation for the gluon distribution,

$$Q^2 \frac{\partial}{\partial Q^2} G(x, Q^2) = \frac{\alpha_s}{2\pi} \int_x^1 \frac{dz}{z} P_{GG}(z) \, G\left(\frac{x}{z}, Q^2\right),$$

with

$$P_{GG}(z) = \frac{2N_c}{z}$$

in the small-x asymptotics but now with *fixed* coupling constant α_s (i.e., for α_s independent of Q^2). In particular show that, in the saddle point approximation, the small-x asymptotics for the gluon distribution is given by

$$x G(x, Q^2) \sim \exp\left(2\sqrt{\frac{\alpha_s N_c}{\pi} \ln \frac{1}{x} \ln \frac{Q^2}{Q_0^2}}\right). \tag{2.159}$$